

LLÉ Review

Quarterly Report



April-June 1983

Laboratory for Laser Energetics
College of Engineering and Applied Science
University of Rochester
250 East River Road
Rochester, New York 14623



LLE Review

Quarterly Report

Editor: J. M. Soures
(716) 275-3866

April-June 1983

Laboratory for Laser Energetics
College of Engineering and Applied Science
University of Rochester
250 East River Road
Rochester, New York 14623



This report was prepared as an account of work conducted by the Laboratory for Laser Energetics and sponsored by Empire State Electric Energy Research Corporation, General Electric Company, New York State Energy Research and Development Authority, Northeast Utilities, The Standard Oil Co. (Ohio), University of Rochester, and various United States Government agencies.

Neither the above named sponsors, nor any of their employees, makes any warranty, express or implied, or assumes any legal usefulness of any information, apparatus, product, or process disclosed, or represents that its use would not infringe privately owned rights.

Reference herein to any specific commercial product, process, or service by trade name, mark, manufacturer, or otherwise, does not necessarily constitute or imply its endorsement, recommendation, or favoring by the United States Government or any agency thereof or any other sponsor.

Results reported in the LLE Review should not be taken as necessarily final results as they represent active research. The views and opinions of authors expressed herein do not necessarily state or reflect those of any of the above sponsoring entities.

IN BRIEF

This issue of LLE Review contains articles on recent progress in the laser fusion effort, on certain aspects of the LLE advanced technology development program, and on National Laser Users Facility activities.

Highlights of the work summarized in this issue include:

- Target design calculations indicating increased drive uniformity and target performance with two-color laser irradiation of directly driven, laser-fusion targets.
- Hydrodynamic efficiency measurements conducted with 351-nm laser irradiation showing a close agreement with predictions made using the two-dimensional hydrodynamic code *SAGE*.
- Continuing theoretical and experimental work aimed at understanding the physical processes taking place in the underdense region of laser-produced plasmas.
- The initiation of x-ray laser experiments on OMEGA.
- The development of liquid-crystal devices as laser-blocking, notch filters.
- The first successful demonstration of single-shot, submicron-resolution, x-ray lithography using a laser-produced plasma as the x-ray source.

CONTENTS

	<i>Page</i>
IN BRIEF	iii
CONTENTS	v
Section 1 LASER SYSTEM REPORT	1
1.A OMEGA Facility Report	1
1.B GDL Facility Report	2
Section 2 PROGRESS IN LASER FUSION	3
2.A Target Designs with Multi-Frequency Irradiation.....	3
2.B Hydrodynamic-Efficiency Measurements on Planar Targets	8
2.C Theory of the Two-Plasmon Decay Instability in a Filament	12
2.D Three-Halves Harmonic Spectra and Self-Focusing in Laser Plasmas.....	19
Section 3 X-RAY LASER EXPERIMENTS	24
Section 4 ADVANCED TECHNOLOGY DEVELOPMENT	30
4.A Liquid-Crystal Laser-Blocking Filters	30
4.B Sub-Micron X-Ray Lithography Using UV-Laser-Produced Plasma as a Source	36
Section 5 NATIONAL LASER USERS FACILITY NEWS.....	40
PUBLICATIONS AND CONFERENCE PRESENTATIONS	43



Laboratory Engineer Kathy Cerqua, of the Optical Materials Group, is shown fabricating a liquid-crystal circular polarizer. The Laboratory for Laser Energetics is carrying out research on the use of liquid-crystal devices in a number of high-power laser applications.

Section 1

LASER SYSTEM REPORT

1.A OMEGA Facility Report

During the third quarter of fiscal year 1983 (April-June 1983) OMEGA facility operations involved (a) the conversion of the laser system for the short-pulse campaign, (b) an x-ray laser campaign, and (c) the manufacturing engineering and equipment installation for the ultra-violet conversion of OMEGA.

Following preparations for the short-pulse campaign in April, we supported the x-ray laser program by verifying the operation of various target diagnostic systems from the Lawrence Livermore National Laboratory (LLNL). Due to the nature of the diagnostics, and the impossibility of cycling targets through a shot without loss of vacuum, the laser system was operated "on demand." The facility was prepared in the early morning and shots taken when the target systems were ready, often late in the evening. During the final week, nearly 24-hour operation was maintained; on the final two days of the campaign, the system was in operation for 32 consecutive hours.

The following is a summary of all activities in OMEGA operations during this quarter:

Target Shots	127
Driver Centering and Calibration	99
Beam Balance	29
Miscellaneous	<u>97</u>
TOTAL	352

In addition, approximately half the operations group was involved, during this quarter, in manufacturing engineering for the upcoming OMEGA frequency conversion. Activities such as parts procurement, tooling, assembly, and component testing continued during this report period. It is noteworthy that despite the high level of system operations the frequency-conversion schedule has been maintained.

With the conclusion of the x-ray laser program, we temporarily suspended OMEGA operations, and began installation of all the components for converting six beams of OMEGA from 1054-nm to 351-nm wavelength. By the conclusion of the quarter, all spatial filters in the converted beams were completed; the large-aperture, optical retarder rails were modified to house frequency conversion crystals; structures for holding beam-diagnostic hardware were in place; one conversion crystal was assembled; and a number of beam transport optics were installed.

1.B GDL Facility Report

GDL operations continued during this quarter. Through April, the laser-matter interaction experiments consisted of hydrodynamic efficiency measurements, Raman scattering, harmonic generation, and a Yale-UCLA NLUF experiment. Shots into the x-ray chamber were taken for both the x-ray devices group and users from the Naval Research Laboratory. A number of shots were used for damage testing.

A summary of GDL operations this quarter follows:

Beta Chamber	102*
X-Ray Chamber	44**
Damage Testing	102
GDL and Miscellaneous	134
	<hr/>
TOTAL	382

*included 23 UCLA/Yale shots

**includes 25 NRL shots.

Section 2

PROGRESS IN LASER FUSION

2.A Target Designs with Multi-Frequency Irradiation

The high-density compressions needed for ICF pellet implosions will require that the nonuniformities in laser-energy deposition not exceed $\sim 1\%$ rms.¹ Differences in energy deposition can cause some regions of the target to be driven harder than others, resulting in shell deformation and ultimately a reduction of neutron yield. The actual amount of nonuniformity which a pellet implosion can tolerate will depend on the details of the individual target, pulse shape, and laser wavelength being used.

Some variance in energy deposition can be smoothed by lateral thermal transport,² while heat is being transported from the region of energy deposition (near the critical surface) to the ablation surface. Long-wavelength laser irradiation can produce substantial amounts of smoothing, because the separation distance, ΔR , between the critical and ablation surfaces increases with wavelength.³ Nevertheless, short-wavelength irradiation (e.g., 351-nm) is preferred for driving fusion targets, due to its higher absorption and hydrodynamic efficiency.⁴ Previous estimates¹ have shown that the smoothing distance, ΔR , achieved by short-wavelength irradiation near the peak of the pulse, should be adequate to smooth the nonuniformities anticipated for ICF reactor illumination.

At the onset of pellet irradiation, the amount of smoothing is expected to be small for all wavelengths; separation between the critical and ablation surfaces is small at this time. One strategy⁵ to

mitigate this "start-up" problem while retaining the benefits of shorter-wavelength irradiation is to illuminate the pellet initially with a longer wavelength (1054-nm), to establish the pellet atmosphere, and then to change to a shorter wavelength to drive the target. The techniques for irradiating a target with different laser frequencies will not be discussed here, but we note that multi-frequency irradiation can occur naturally by tripling the frequency from Nd:glass lasers.⁶ When tripling crystals are optimized to produce blue light (351-nm) at the high-intensity peak of the pulse, the conversion efficiency will be poor at low intensity, resulting in irradiation predominantly with red light (1054-nm) at the start of the pulse.

We have begun one- and two-dimensional computer simulations to determine a pellet's tolerance to imposed irradiation nonuniformities with and without multi-frequency illumination. The numerical simulations were carried out on the cryogenic target shown in Fig. 1. This target is composed of a polyethylene (CH₂) ablator and solid D-T fuel. The pellet was irradiated with the double-Gaussian pulse shown in Fig. 2, containing approximately 30 kJ of energy. The pulse-timing was chosen so that the target reaches the energy break-even point for uniform irradiation at normal incidence. (Note that this is not necessarily an optimal design for 30 kJ and no attempt has been made to examine its hydrodynamic stability.) Numerical simulations were performed for two cases: one in which both pulses of the double-Gaussian pulse were blue and the other for which the first pulse was red and the second blue.

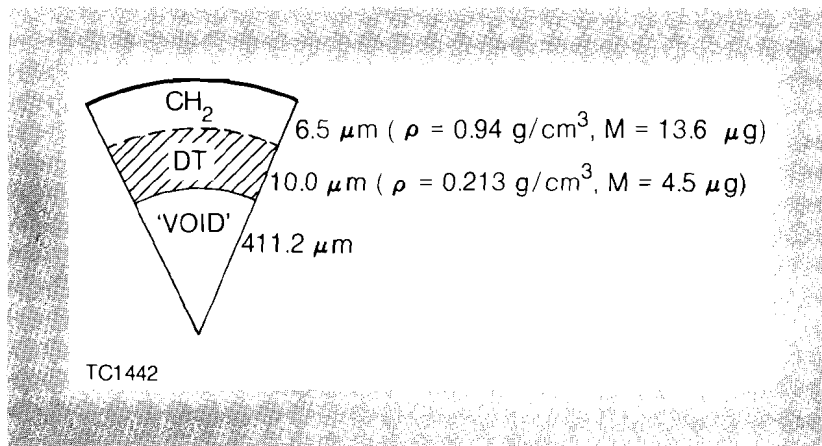
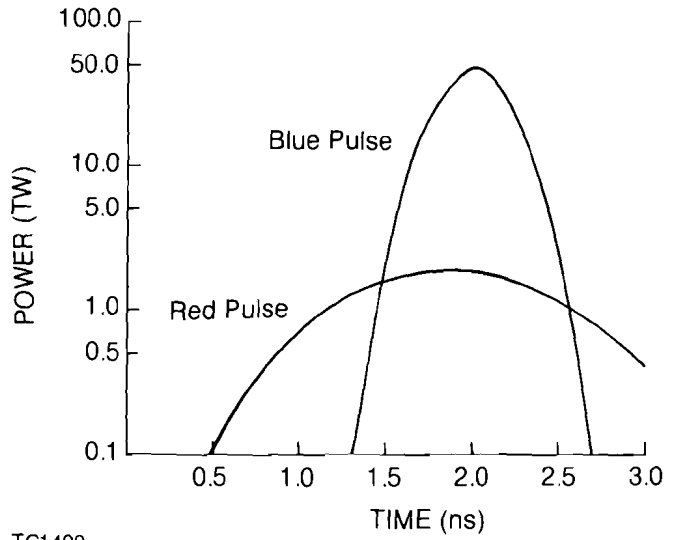


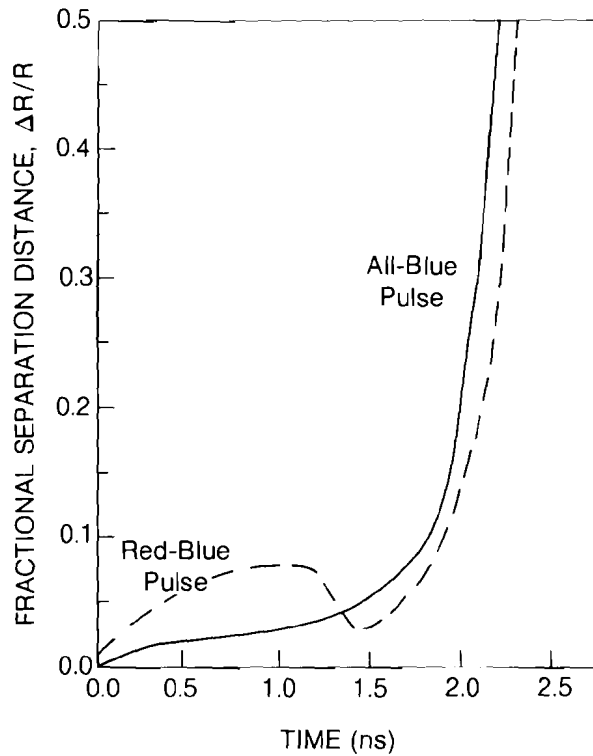
Fig. 1
Cryogenic target used to model shell deformation by nonuniform laser irradiation.

The fractional separation distance, ΔR , between the critical and ablation surfaces is plotted as a function of time during the implosion on Fig. 3 for the two cases considered. This factor, in part, determines the amount of thermal smoothing. The attenuation of the nonuniformity in laser-energy deposition may be expected to vary as $\exp(-l\Delta R/R)$ where l is the mode number in a spherical harmonic decomposition of the nonuniformity. (The spatial wavelength λ of the nonuniformity is related to l and the target radius R by: $\lambda = 2\pi R/l$.) Previous calculations¹ have shown that a value $\Delta R/R \approx 0.1$ should be adequate for smoothing the nonuniformities characteristic of an ICF-reactor laser configuration; this is because of the high degree of uniformity in laser deposition and the small spatial wavelength of the nonuniformity ($l \geq 10$). As seen in Fig. 3, $\Delta R/R = 0.1$ is reached before the peak of



TC1490

Fig. 2
 Double-Gaussian pulse used in the calculations. The effect on the implosion of a red or blue first pulse was examined.



TC1493

Fig. 3
 Calculated smoothing distance between the critical and ablation surfaces as a function of time for the all-blue and red-blue cases. Note the increased smoothing distance for the red-blue combination early in time.

the pulse; thus, most of the laser energy should be absorbed with relatively good smoothing. The large values of $\Delta R/R$ achieved at the peak of the pulse are due to a reduction in target radius during the implosion. At the onset of irradiation, there should be negligible smoothing for the all-blue pulse. Although only a small amount of energy is deposited early in time, it is possible to generate a shock at the ablation surface which will travel through the target and imprint the laser nonuniformity directly on the fuel.

The increased smoothing distance achieved with the red prepulse is evident in Fig. 3. Although the value reached during the first pulse, $\Delta R/R \sim 0.07$, is not large due to the low intensity, it could be adequate for smoothing an $\ell = 10$ nonuniformity by a factor of 2. The decrease in $\Delta R/R$ for the red-blue pulse relative to the all-blue pulse at ~ 1.5 ns is not significant and results from a slight difference in the implosion times.

To examine the effect of laser nonuniformity on the target implosion, two-dimensional simulations were performed with the Lagrangian code *ORCHID* in which an $\ell = 8$ variation was superimposed on the laser power (assuming normal incidence). The peak-to-valley variation of laser intensity was 4%, corresponding to $\sigma_{rms} = 1\%$. The deformation of the shell was measured in terms of the distortion of numerical grid interfaces, $R(\theta)$, at different places in the target, with the rms variation defined as:

$$\delta_{rms} \equiv \frac{1}{\pi} \frac{\int [R^2(\theta) - \langle R \rangle^2]^{1/2} d\theta}{\langle R \rangle}$$

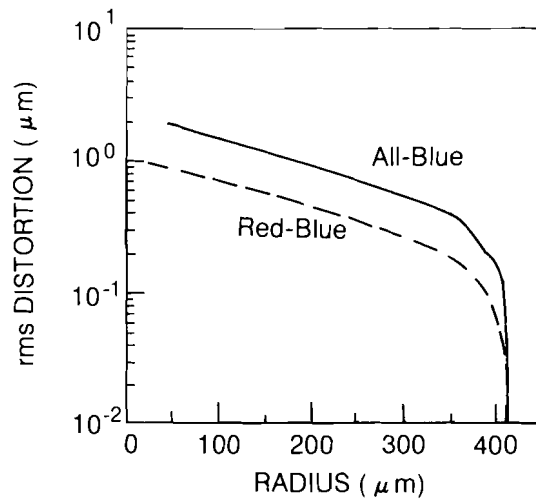
where

$$\langle R \rangle = \frac{1}{\pi} \int R(\theta) d\theta .$$

Figure 4 shows how the rms variation of an interface near the center of the fuel changes during the implosion for both the all-blue and the red-blue pulses.

The onset of deformation occurs at the initial shell radius of $\sim 400 \mu\text{m}$ as the laser nonuniformity imprints itself on the target. The deformation then increases by an order of magnitude during the remainder of the implosion. Such a sudden onset of the deformation when the shell first begins to move is similar to results discussed in Ref. 7. As seen, the distortion produced in the target by the red-blue pulse is less by a factor of two.

The reasons why this particular target can tolerate more of the laser nonuniformity with the red-blue combination have not been completely determined. Two factors were observed in the simulations: one was the increased smoothing distance produced by the red prepulse; second, the red light was found to produce a weaker "first shock," resulting in less preheat and less decompression of the fuel. We are currently investigating the influence these two factors have on the target implosion.



TC1491

Fig. 4

Growth of target deformation during the implosion. The target can tolerate about a factor of 2 more laser nonuniformity using the red-blue pulse.

REFERENCES

1. S. Skupsky, R. L. McCrory, R. S. Craxton, J. Delettrez, R. Epstein, K. Lee, and C. Verdon, "Uniformity of Energy Deposition for Laser-Driven Fusion," Laboratory for Laser Energetics Report No. LLE-138. To be published in *Laser Interaction and Related Plasma Phenomena*, edited by H. Hora and G. Miley (Plenum Press, New York, 1983).
2. M. H. Emery, J. H. Orens, J. H. Gardner, and J. P. Boris, *Phys. Rev. Lett.* **48**, 253 (1982).
3. J. H. Gardner and S. E. Bodner, *Phys. Rev. Lett.* **47**, 1137 (1981).
4. R. L. McCrory and R. L. Morse, *Phys. Rev. Lett.* **38**, 544 (1977).
5. J. H. Nuckols, "Laser-Induced Implosion and Thermonuclear Burn," *Laser Interaction and Related Plasma Phenomena*, edited by H. Schwarz and H. Hora (Plenum Press, New York, 1974), Vol. 3B, pp. 399-425.
6. W. Seka, S. D. Jacobs, J. E. Rizzo, R. Boni, and R. S. Craxton, *Opt. Commun.* **34**, 469, (1980); R. S. Craxton, *ibid.* **34**, 474 (1980).
7. W. C. Mead and J. D. Lindl, "Symmetry and Illumination Uniformity Requirements for High-Density, Laser-Driven Implosions," Lawrence Livermore National Laboratory Report No. UCRL-78459, 1976.

2.B Hydrodynamic-Efficiency Measurements on Planar Targets

The efficiency with which the laser energy absorbed by the plasma is transferred to the compressed core is one of the most important parameters in laser-driven fusion. Since this quantity is very difficult to deduce experimentally in spherical geometry, we have conducted a series of experiments using planar targets to assess our ability to make accurate predictions of this efficiency. We describe here a set of experiments using thin, planar targets illuminated by 351-nm and 1054-nm laser light, in which we have measured the kinetic energy of the accelerated target mass on the rear side of the target (opposite to the laser).

When using planar targets, one prefers to use sufficiently large spot sizes so that the acceleration is essentially one-dimensional. This condition would require the use of spot sizes greater than $200\ \mu\text{m}$ in radius, and irradiation intensities below $10^{13}\ \text{W}/\text{cm}^2$, since we unfortunately have only 50-60 J available in one UV beam. These intensities are too low for our future needs, so we chose to use smaller spot sizes, of radius 50-200 μm , and set out to account for the non-planar nature by comparing the experimental results with two-dimensional hydrodynamic computations carried out with the Eulerian code *SAGE*.¹ As will be seen, the agreement between the experimental observations and the predictions of the computer code permits us to interpret these experiments with a certain degree of confidence.

Planar CH foils were irradiated with 1-ns pulses of 351-nm light at intensities typically around $10^{14}\ \text{W}/\text{cm}^2$, but in some cases as high as $7 \times 10^{14}\ \text{W}/\text{cm}^2$. The kinetic energy of the unablated target mass was measured on the rear side of the target using two types of plasma calorimeters. One is a relatively small, compensating calorimeter. Because of their small size and their ability to discriminate between plasma and light energy, these devices were used near the target normal at angles out to 32° . Above 32° , the small calorimeters were not sensitive enough to record the low-amplitude signals. Large-aperture calorimeters were used to cover the angular region above 32° . These measurements allow one to measure the integrated energy above 32° but give very little angular resolution. Thus, we may compare the predicted and observed angular distributions up to 32° and the total energy integrated over all angles.

Very strong angular effects associated with small spot sizes are evident in the calculated angular distributions of Fig. 5. In these calculations, inverse-bremsstrahlung absorption was assumed to be the only absorption mechanism, and a thermal-conduction flux limiter of $f = 0.04$ was used. One notes that for spots of radius $200\ \mu\text{m}$ or greater, almost all the energy is in the forward direction, i.e., normal to the surface. Thus, a one-dimensional planar approximation would be reasonable for such spots. For $120\text{-}\mu\text{m}$ -radius spots, the contributions at angles greater than 10° are already significant, and for radii less than $80\ \mu\text{m}$ the expansion is strongly divergent rather than planar.

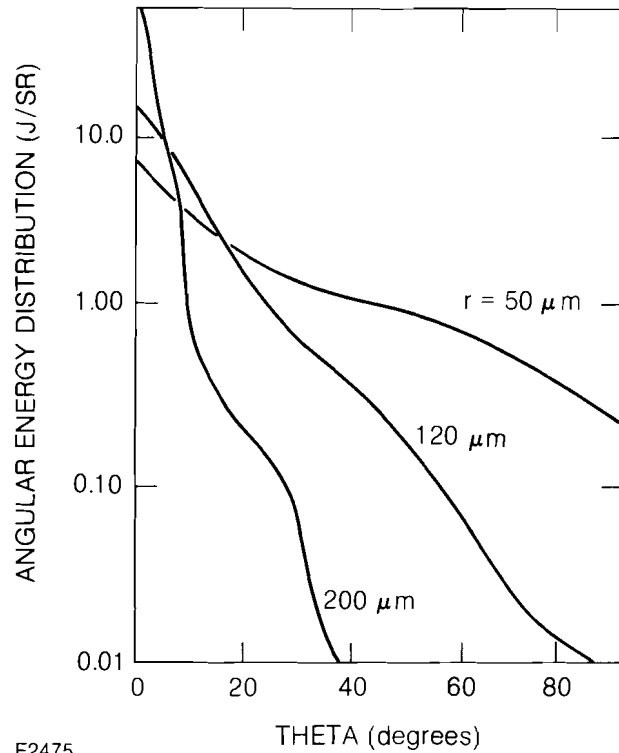


Fig. 5
Predictions of the code SAGE for the angular energy distribution of the rear plasma blow-off from CH targets irradiated with various spot sizes. Simulations are for 351-nm, 40-J, 1-ns pulses on 10- μm CH targets. The blow-off changes from highly planar to strongly divergent as the spot size decreases.

Figures 6a and 6b show the satisfactory agreement between the observed and predicted angular distributions for 50- μm - and 100- μm -radius spots.

The experimental data for the 100- μm -radius case are adequately modeled by using the 120- μm -radius code calculation. We have determined that the intensity distribution changes from nearly Gaussian at best focus to a ring-like structure at larger spot radii. The 100- μm -radius spot is located just below the transition region. As shown, the code can satisfactorily model the shots with small spots using a uniform intensity distribution. However, in modeling shots with a radius greater than 200 μm the code predicts planar-like blow-off, whereas in the experiment the blow-off still retains its divergent nature. We have found that the intensity distribution can affect the shape of the rear blow-off. Small-scale beam intensity variations can accelerate material a distance comparable to the local intensity scale length during the laser pulse. The result is a locally divergent expansion which will affect the overall shape of the blow-off. Code calculations for a ring intensity distribution demonstrate this result. Figure 7a shows density contour plots and ray trajectories for a uniform intensity distribution at two different times during the irradiation. Figure 7b shows similar data using a ring intensity distribution. The annular ring leads to a more divergent expansion, contributing to significant amounts of energy at large angles with respect to the target normal.

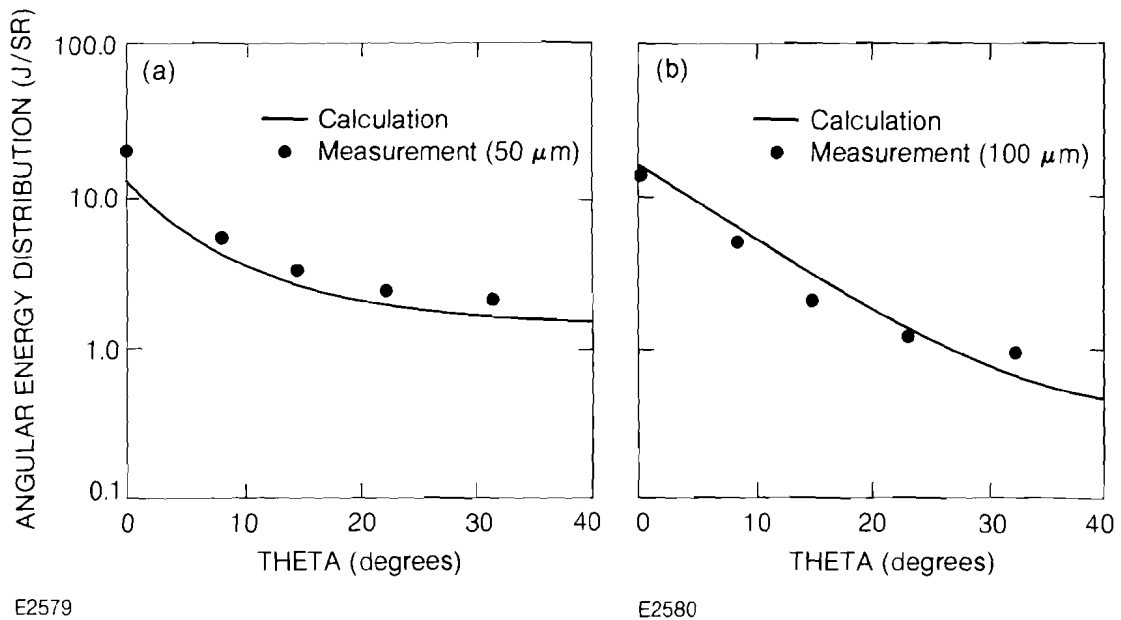


Fig. 6
Comparison between code predictions and experiments for the rear plasma energy distribution for (a) small (50- μm radius) spots and (b) 100- μm spots. The 10- μm -thick CH targets are irradiated with 1-ns pulses of 351-nm light. [In case (b) a spot radius of 120 μm was assumed in the calculation.]

The ability to model large-spot experiments correctly depends on the ability to characterize the intensity distribution of the focal spot.

Figure 8 shows the measured hydrodynamic efficiency (plasma kinetic energy divided by absorbed energy) versus absorbed intensity for constant target thickness and for 351-nm and 1054-nm irradiation. The absorption fractions used in order to plot the experimental data were taken from LLE measurements on thick plastic targets for 351-nm radiation,² and from the SAGE calculations for 1054-nm radiation.

A close correlation is seen in Fig. 8 between the observed and calculated efficiencies, at both wavelengths and across a broad intensity range. The agreement at the high-intensity end of the 351-nm curve should, however, be treated with caution, since the code predicts significant transmission of laser energy ($>8\%$ at incident intensities above $3 \times 10^{14} \text{ W/cm}^2$) which has not been observed in these experiments.

Caution should also be exercised in comparing the hydrodynamic efficiencies measured at the two different wavelengths: on account of the much-reduced mass-ablation rate at 1054 nm, the 10- μm target thickness was above the optimum for 1054-nm radiation. It is still worth noting that, for 351-nm radiation and at incident intensities a few times 10^{14} W/cm^2 (where the absorption efficiency is $\approx 80\%$), $\sim 20\%$ of the incident energy may be converted into kinetic energy of the accelerated target.

Finally in Fig. 9 we show the variation of the hydrodynamic efficiency with target thickness keeping the intensity constant (at

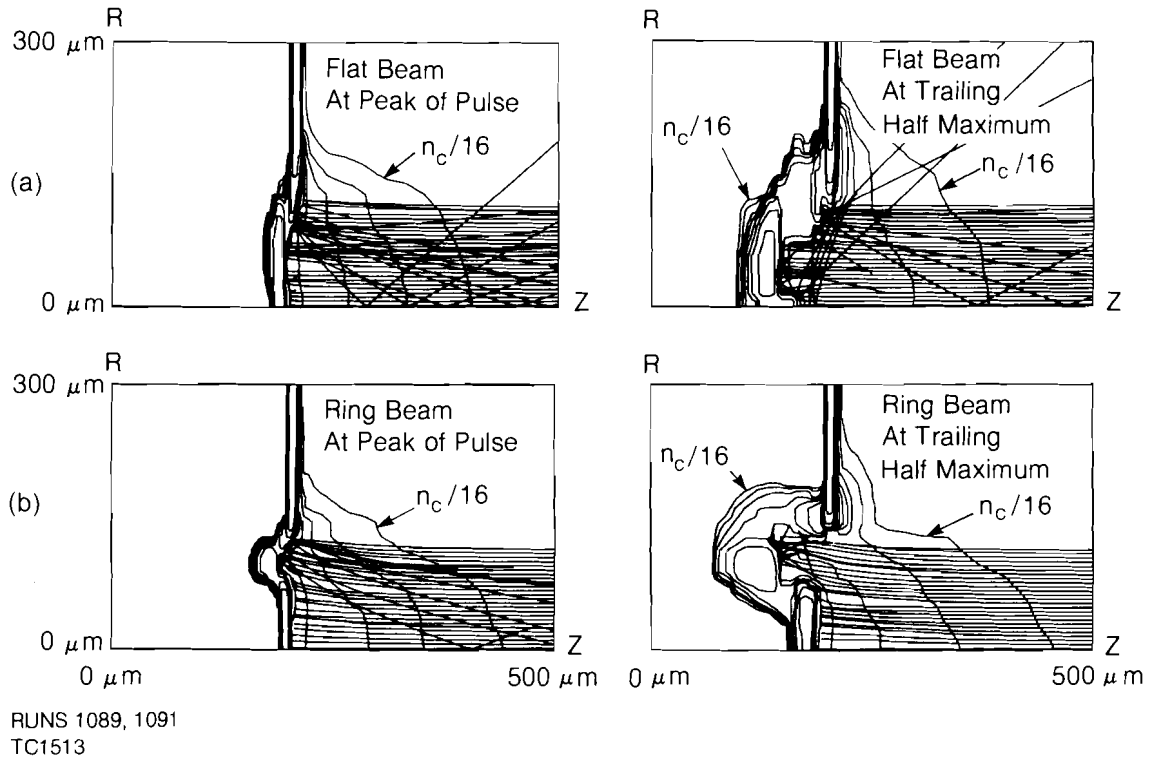
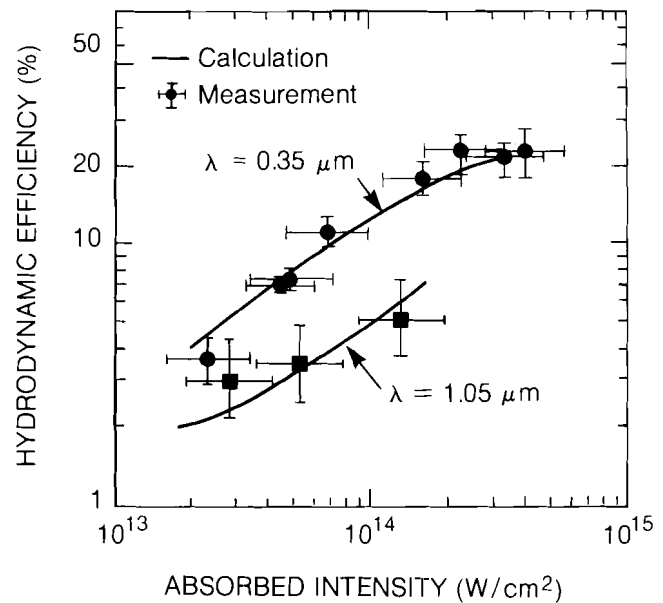


Fig. 7
 Electron density contours and ray trajectories calculated by SAGE for 10- μm CH targets irradiated with 1-ns pulses of 351-nm light. The density changes by a factor of 2 between contours. The effect of the focal-spot intensity distribution on the rear blow-off is shown by comparing (a) a uniform intensity distribution at $7.2 \times 10^{13} \text{ W/cm}^2$ and (b) a ring distribution with a 5:1 (1×10^{14} : $2 \times 10^{13} \text{ W/cm}^2$) intensity ratio. Both simulations are for a 10- μm -thick CH target; the contours shown are at the peak and trailing half-maximum of a 1-ns pulse for both cases.

Fig. 8
 Comparison of measured and predicted hydrodynamic efficiency for 10- μm CH targets for various absorbed intensities. The hydrodynamic efficiency is defined relative to the absorbed energy.



E2582

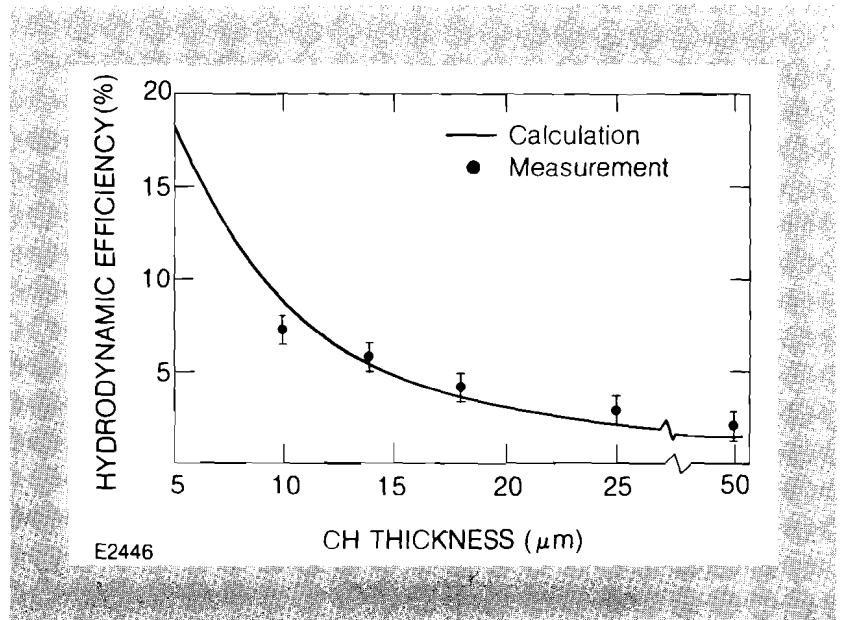


Fig. 9
Dependence of hydrodynamic efficiency on the thickness of CH targets for a constant intensity of $7.2 \times 10^{13} \text{ W/cm}^2$ and a pulse width of 1 ns.

$7.2 \times 10^{13} \text{ W/cm}^2$). Again the agreement between the measured and the calculated values is close.

The major conclusion to be drawn from these experiments is that finite size targets may be used for hydrodynamic-efficiency measurements provided one properly takes into account the two-dimensional properties of the accelerated expansion.

REFERENCES

1. R. S. Craxton and R. L. McCrory, Laboratory for Laser Energetics Report No. 99 (1980); R. S. Craxton and R. L. McCrory, Laboratory for Laser Energetics Report No. 108 (1980).
2. W. Seka, R. S. Craxton, J. Delettrez, L. Goldman, R. Keck, R. L. McCrory, D. Shvarts, J. M. Soures, and R. Boni, *Opt. Commun.* **40**, 437 (1982).

2.C Theory of the Two-Plasmon Decay Instability in a Filament

Discrepancies between predictions of the conventional model of the two-plasmon decay and experimental observations of $3\omega_0/2$ spectra have led to consideration of a new model, where the decay occurs inside a filament. Predictions of the new model agree well with observations.

Of the various parametric instabilities which can be generated by laser light propagating through the corona, the two-plasmon decay instability (TPD) is one of the most difficult to diagnose. This problem arises because in TPD an incident photon decays into two plasma waves (plasmons) which are confined to the plasma, and thus cannot

be directly observed. The occurrence of the decay may be inferred from Thompson-scattering of a probe laser beam from the decay plasmon;¹ however, the simplest experimental signature is the generation of half-integer harmonic light at frequencies $\omega_0/2$, $3\omega_0/2$, etc. (where ω_0 is the frequency of the laser) by interaction of the decay plasmons with incident laser photons. The generation of the $3/2$ harmonic is the easiest to understand, since it simply involves the "addition" of a plasmon of frequency $\sim \omega_0/2$ and a laser photon of frequency ω_0 . The generation of $\omega_0/2$ light is more complicated, since it is produced not only by "subtraction" of a plasmon from an incident photon, but also by linear conversion of the decay plasmons to photons and by absolute Raman scattering.

The dispersion relation for plasma waves may be written

$$\omega^2 = \omega_p^2 [1 + 3(k\lambda_D)^2] \quad (1)$$

where ω , k are the plasmon frequency and wave vector, respectively, ω_p is the local plasma frequency, and λ_D is the Debye length. Landau damping of short-wavelength plasmons imposes the restriction $k\lambda_D \leq 0.2$, so Eq. (1) implies that $\omega^2 \approx \omega_p^2$. Thus, both plasmons in TPD must have frequencies approximately equal to ω_p . Since the sum of the two frequencies must equal ω_0 , we see that the decay occurs for $\omega_p \approx \omega_0/2$, or where the density is one-quarter of critical density.

TPD has usually been thought to occur at the quarter-critical surface of the bulk plasma density profile. To first approximation, this surface may be regarded as a plane perpendicular to the wave vector \mathbf{k}_0 of the incident light. The sum of the wave vectors of the two TPD plasmons must equal \mathbf{k}_0 , and so they must have equal and opposite values of \mathbf{k}_\perp , the component of \mathbf{k} perpendicular to \mathbf{k}_0 . The sum of the frequencies of the two plasmons must equal ω_0 , and so one has frequency $\omega_0/2 + \Delta$ and the other $\omega_0/2 - \Delta$. As explained in Ref. 2, the modes with maximum growth rate are determined by a hyperbola in \mathbf{k} -space; for these modes Δ is a function only of $|\mathbf{k}_\perp|$. When one of these plasmons is added to a laser photon to produce a $3\omega_0/2$ photon, the entire perpendicular component of the $3\omega_0/2$ photon wave vector must come from the plasmon: $(\mathbf{k}_{3/2})_\perp = (\mathbf{k})_\perp$. Since the density gradient is parallel to \mathbf{k}_0 , \mathbf{k}_\perp is conserved in the propagation of plasmons and photons, and it is this \mathbf{k}_\perp which determines the angle θ at which the $3\omega_0/2$ photon is observed:

$$\sin\theta = \frac{1}{\sqrt{3}} \left| \frac{k_\perp}{k_0} \right|.$$

The spectral splitting Δ for these modes is

$$\Delta = \frac{3v_1^2 k_0^2}{2\omega_0} \sqrt{1 + 12 \sin^2\theta}. \quad (2)$$

Thus, at a given angle of observation θ , we expect to see two peaks in the $3\omega_0/2$ spectrum, shifted symmetrically by $\pm\Delta$ from the exact $3\omega_0/2$ frequency. This is consistent with experimental data at 1054-

nm; however, in experiments performed with 351-nm laser light the two peaks are always shifted asymmetrically, with the red shift two to three times larger than the blue shift. The strong angular dependence of the shift, predicted by Eq. (2), is not seen; the splitting is essentially independent of the angle of observation.

To explain these observations, a new model has been developed as shown in Fig. 10. We assume that, due to self-focusing, hot spots in the incident beam form small cylindrical channels in the plasma ("filaments") in which the central density is much lower than the background density n_0 outside the filament. If n_0 is larger than one-fourth of critical density, a cylindrical quarter-critical surface can be formed inside the filament, at which TPD can occur. For a linearly polarized pump, there exist regions of both s- and p-polarization in the filament, as shown.

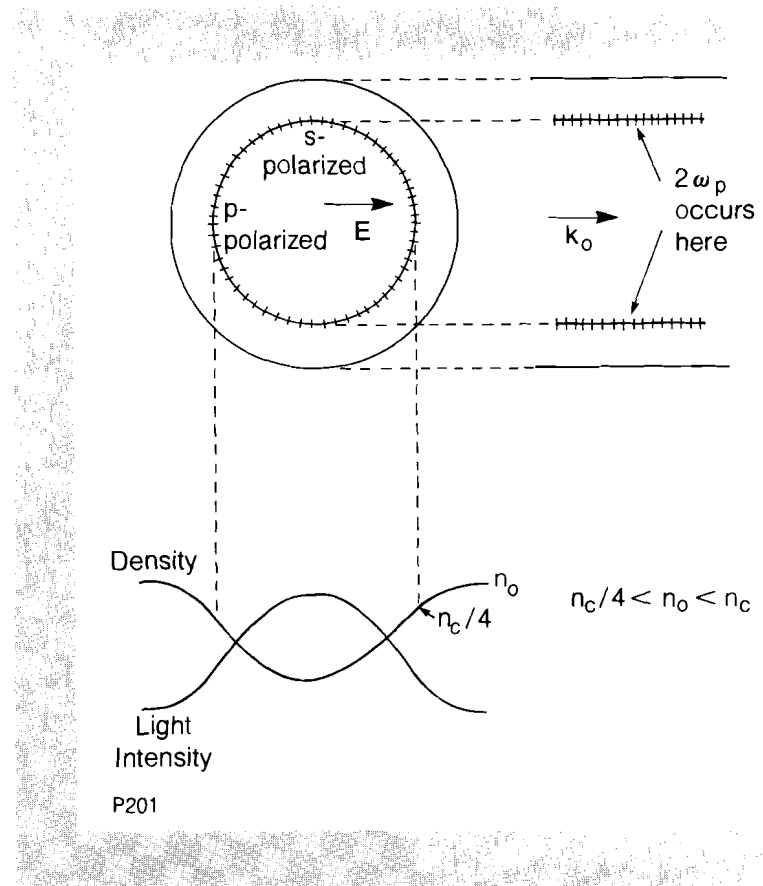
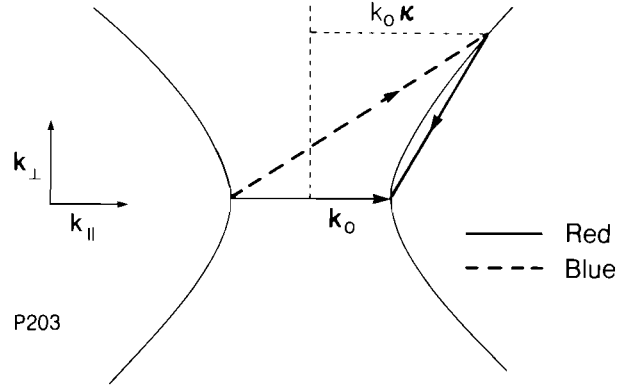


Fig. 10
Geometry of filament and quarter-critical surface. The hash marks show the quarter-critical region where two-plasmon decay occurs. The background plasma density is n_0 , the wave vector of the light in the filament is k_0 , and n_c is the critical density.

To calculate approximate thresholds and growth rates for TPD in a filament, we use a simplified model, where we neglect the curvature of the filament wall (which should be valid for filament radii much larger than a wavelength) and the radial variation of the laser-light intensity (which is small over the region near quarter-critical where TPD is localized.) We first determine modes of the homogeneous problem which are absolute in the directions perpendicular to k_0 , so that they do not propagate away from quarter-critical density. These modes are determined by a hyperbola in k -space, as shown in Fig. 11, and also happen to be the modes with the largest growth rate.² The parameter κ

Fig. 11

Modes in homogeneous plasma which are non-propagating in directions perpendicular to the incident light wave vector k_o . Each point on the hyperbola represents the apex of a decay triangle, with the two-plasmon wave vectors adding to give k_o . The plasmon frequency shifts from the exact half-harmonic are proportional to the parameter κ , which is defined as the distance from a line bisecting k_o to the apex of the decay triangle measured in units of k_o .



determines the frequency shift of the two plasmons from $\omega_o/2$; κ is $1/2$ at the tip of the hyperbola and increases with larger wave vector plasmons. The effect of the radial density inhomogeneity may be obtained through a perturbation approach based on a WKB analysis of the Fourier-transformed plasma-wave equations³; the resulting frequencies are

$$\frac{\omega}{\omega_o} = \frac{1}{2} \pm 3 \frac{v_T^2 k_o^2}{\omega_o^2} \kappa + i \frac{2}{3} \frac{k_o v_o}{\omega_o} \left(1 - \frac{1}{\alpha \kappa}\right) \quad \text{p-polarized}$$

$$\frac{\omega}{\omega_o} = \frac{1}{2} \pm 3 \frac{v_T^2 k_o^2}{\omega_o^2} \kappa + i \frac{2}{3} \frac{k_o v_o}{\omega_o} \left(1 - \frac{1}{\alpha \sqrt{\kappa^2 - 1/4}}\right) \quad \text{s-polarized}$$

where $\alpha \equiv 4(k_o v_o / \omega_o) k_o L$, v_o is the electron quiver velocity in the laser field, v_T is the electron thermal velocity, and L is the radial-density scale length. The second term on the right is the frequency shift, proportional to κ , and the last term is the growth rate. Instability requires $\alpha \kappa > 1$; by choosing modes with k (and therefore κ) large enough this condition can always be satisfied. However, Landau damping limits the size of k , requiring $k \lambda_D \leq 0.2$. This yields a threshold condition:

$$\frac{v_o}{v_T} k_o L > 3$$

In a filament we expect the ponderomotive force to essentially balance the thermal pressure force, and so we have $v_o / v_T \sim 1$. Also, the radial-density scale length should be one wavelength or longer, and so $k_o L \sim 2\pi L / \lambda_o \leq 2\pi$. Thus, the condition (Eq. 3) for TPD in a filament is readily satisfied.

In Fig. 12 we illustrate how the red-shifted $3\omega_o/2$ component is produced in a filament. A red-shifted plasmon propagates in the radial density profile until its wave vector is appropriate to add to k_o to produce the wave vector of a $3\omega_o/2$ photon. To produce this light in

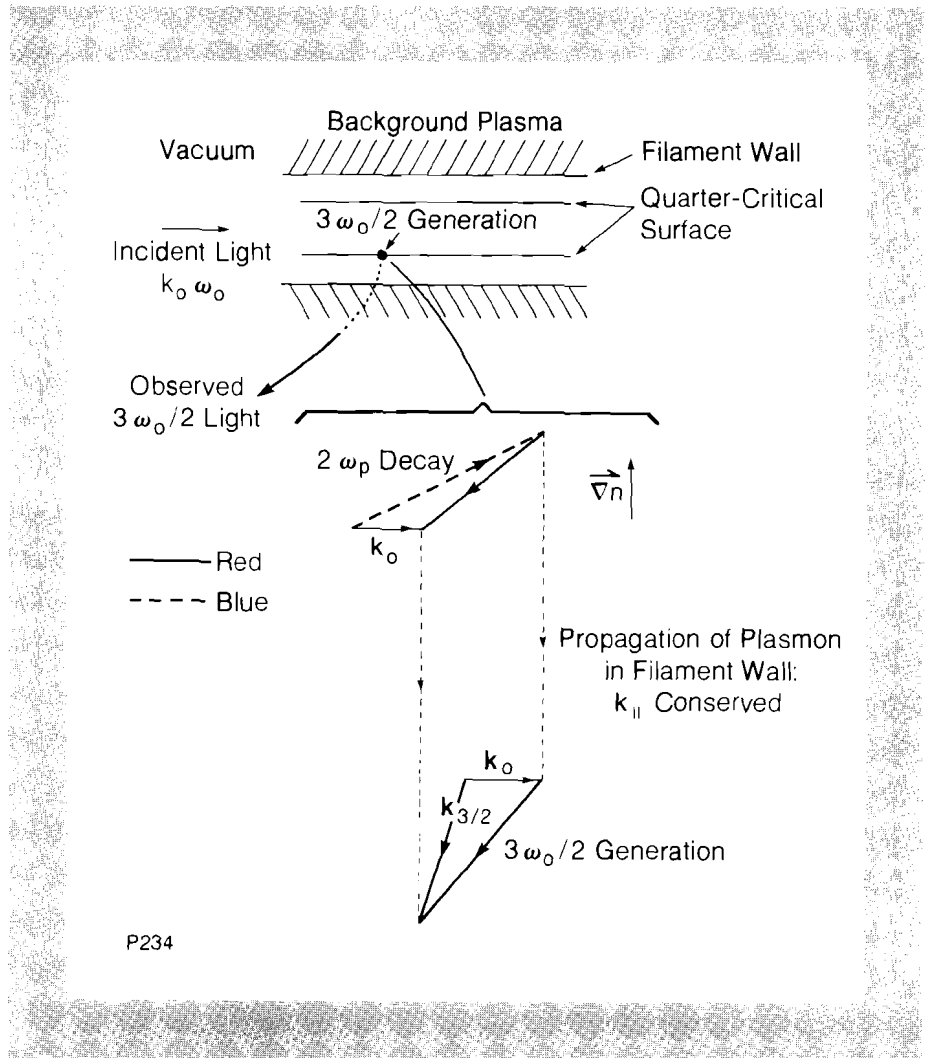


Fig. 12
 Generation of 3/2-harmonic in a filament. The blow-up shows \mathbf{k} -matching conditions for the generation of red-shifted back-scattered 3/2-harmonic, as explained in text. The vector ∇n represents the radial-density gradient; the axial component of the plasmon wave vector, k_{\parallel} , is conserved as the plasmon propagates in the filament.

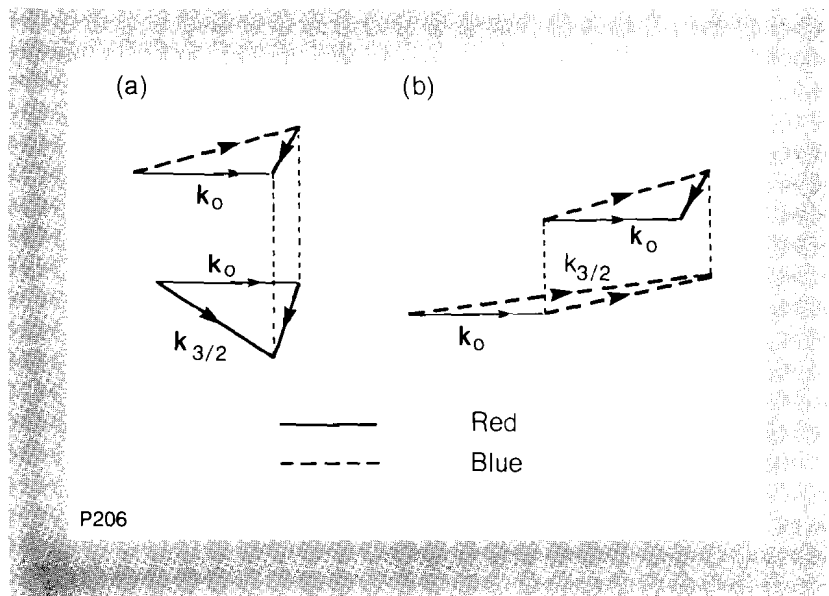
the backward direction, as shown here, \mathbf{k} must be fairly long in order to cancel the forward-directed \mathbf{k}_0 . Thus, these decays have large κ 's and large red shifts. Red plasmons from decays with smaller κ 's, and, thus, smaller red shifts, produce a red $3\omega_0/2$ peak in a range of angles in the forward direction, as shown in Fig. 13a. However, since $k_{3/2} > k_0$, $k_{3/2}$ must have a significant perpendicular component, and, thus, red-shifted $3\omega_0/2$ light is excluded from a cone angle of about 20° around the forward direction.

In Fig. 13b, we see the generation of blue-shifted $3\omega_0/2$ radiation. Since the blue plasmon has a k_{\parallel} greater than k_0 , the requirement that the sum of the blue plasmon and photon wave vectors yield a $3\omega_0/2$ wave vector means we must have $2k_0 < k_{3/2}$. Now \mathbf{k}_0 is the photon wave vector inside the filament, and its exact value depends on the detailed radial-density profile of the filament. However, \mathbf{k}_0 becomes smaller as the background density n_0 outside the filament becomes larger (larger background densities decrease the filament radius and increase the average radial density, both of which tend to decrease \mathbf{k}_0). If we take \mathbf{k}_0 to be the wave vector of laser light in the background

Fig. 13

a) Wave-vector matching diagram for generation of red forward-scattered $3/2$ -harmonic. The maximum component of $k_{3/2}$ in the forward direction is k_0 , and so the red-shifted $3/2$ -harmonic cannot be generated within a cone of about 20° around the forward direction.

b) Wave-vector matching for the blue-shifted $3/2$ -harmonic. Generation of this light is limited to angles near the forward direction.



plasma we get a necessary condition that $n_0 > 7/12 n_c$ for wave vector matching; a sufficient condition for blue $3\omega_0/2$ generation may require even larger n_0 . Thus, we see that blue-shifted $3\omega_0/2$ light should be produced only at background densities near critical. From the diagram we also see that blue $3\omega_0/2$ is generated only in directions close to the forward direction; because of this fact and the high background density, the $3\omega_0/2$ will tend to remain confined to the filament. Finally, the blue plasmons which create $3\omega_0/2$ light have small values of κ ($\kappa \sim 1/2$), so the blue shifts should be relatively small.

Figures 14 and 15 show the consequences of this model for overdense and underdense planar target experiments, respectively. In Fig. 14, the overdense case, we see that both red and blue $3\omega_0/2$ light is spread over a wide range of angles, in such a way that the angular dependence of the spectral shifts should be eliminated. In the underdense case (Fig. 15) the red-light angular dependence is also lost, though we expect the forward-scattered light to show a smaller red shift than the backscattered $3\omega_0/2$, and we also expect red light to be excluded from the forward direction. Since the filament can extend through the underdense plasma, the blue light remains confined throughout the filament and emerges in a small cone around the forward direction. Two observations of this forward-scattered light are indicated here, one of which (LLE) at 135° saw only red light, while the other at Livermore, an observation with 1060-nm incident light at $\sim 150^\circ$, saw only blue light, in accordance with our theory (Sec. 2.D, Ref. 3).

In short, we have shown that the threshold condition for the occurrence of TPD in filaments is readily satisfied. For overdense target experiments, the resulting $3\omega_0/2$ emission spectrum should have two peaks, one shifted to the blue and the other shifted two to three times farther to the red from the exact $3\omega_0/2$ frequency. The splitting should show little dependence on angle of observation. For underdense planar targets, the red peak should have a larger shift in

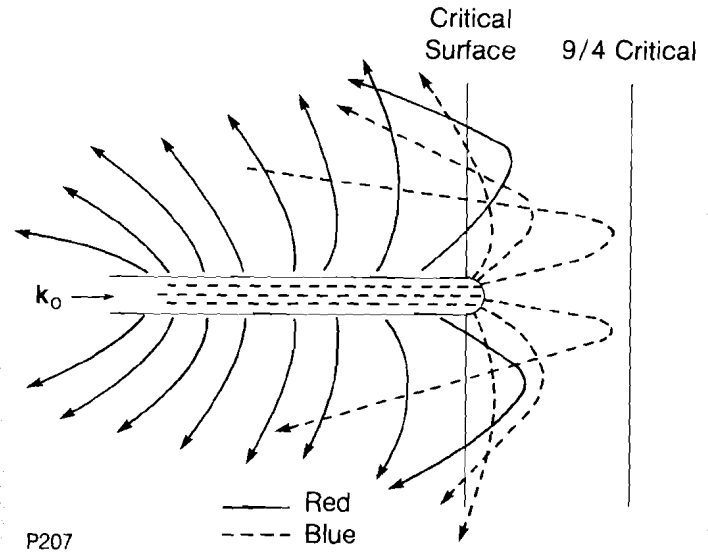


Fig. 14
 Generation of 3/2-harmonic by filaments in underdense plasma target. Both red and blue components are scattered widely, so that the angular dependence of the spectral splitting is largely averaged out.

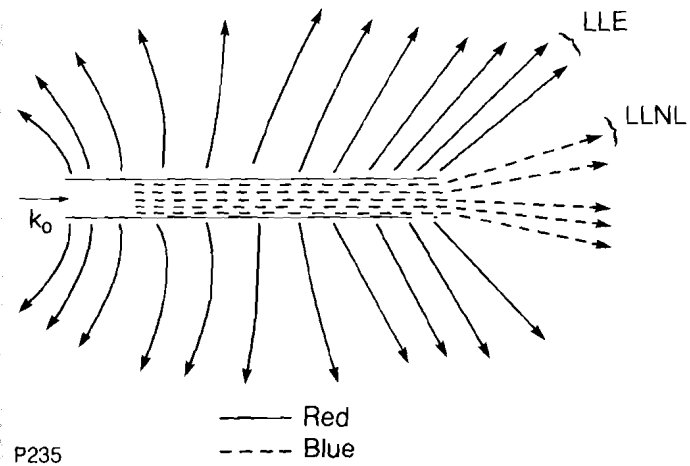


Fig. 15
 Generation of 3/2-harmonic by a filament in an underdense planar target. Blue-shifted light is confined to narrow forward cone; red-shifted light is excluded from forward direction. These features of forward-scattered 3/2-harmonic shown are discussed in the text.

backscatter than in forward scatter, and should be excluded from a cone of about 20° around the forward direction. The blue peak should be seen only very near the forward direction. These predictions seem to agree well with experimental observations so far; further experiments are planned to test the theory more thoroughly.

REFERENCES

1. H. A. Baldis and C. J. Walsh, *Phys. Fluids* **26**, 1364 (1983).
2. LLE Review **14**, Section 2.B (1982).
3. C. S. Liu and M. N. Rosenbluth, *Phys. Fluids* **19**, 967 (1976).

2.D Three-Halves Harmonic Spectra and Self-Focusing in Laser Plasmas

We have recently reported on the spectral characteristics and the generation mechanisms for the harmonic radiation emitted from laser-produced plasmas.¹ We noted on that occasion that the observed asymmetric splitting of the $3\omega_0/2$ spectra from UV-laser plasmas (Fig. 16) could not be explained on the basis of a planar plasma-expansion model. In the preceding article of this review, the theoretical basis has been laid for the two-plasmon decay instability (TPD) inside filaments formed by the incident laser in the plasma corona. In this article we present some experimental data recently obtained on thin plastic targets irradiated at 351 nm at intensities of up to 10^{15} W/cm² on the UV irradiation facility, GDL.

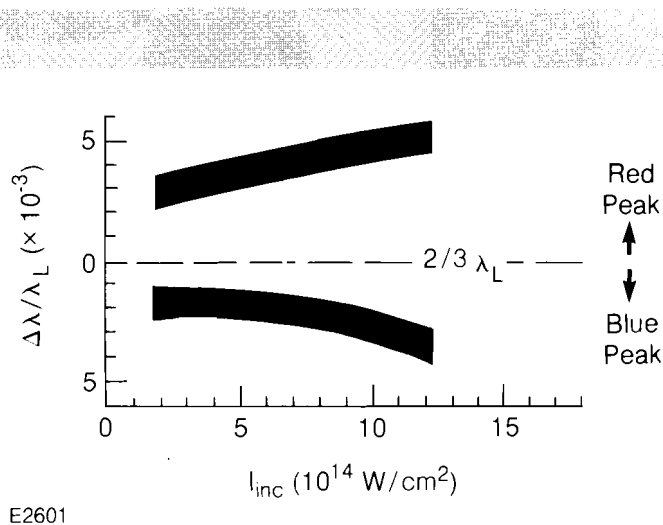


Fig. 16
Intensity dependence of the spectral splitting of the $3\omega_0/2$ radiation emitted from planar UV plasmas. We note the strong asymmetry of the splitting which cannot be modeled by conventional theory applied to planar targets. The data were taken with 0.5 ns at $\lambda_L = 351$ nm. Irradiated spot radius ranged from $50 \mu\text{m}$ to $200 \mu\text{m}$. The targets were thick CH foils.

The existence of the filamentation of the incident laser light in the corona of laser plasmas has been known for some time. Experiments employing visible shadowgraphy have revealed evidence for filamentation under certain irradiation conditions.² At LLE, we do not have any direct evidence of filamentation. Indirect evidence for filamentation exists in some of the single-beam, planar target experiments conducted with the GDL laser. Furthermore, there is some evidence that nonlinear interaction mechanisms such as the two-plasmon decay (TPD) instability, observed in these one-beam experiments, occurs predominantly in filaments. In this article we present some spectroscopic data related to the preceding theoretical article on TPD inside filaments.

In experiments on thin plastic foils, irradiated in GDL with a single UV beam, we have observed the $3\omega_0/2$ spectra around 234 nm in several different angular directions: in backscattering through the focusing lens, at 45° , and in forward scattering at 135° with respect to the incident light (45° with respect to the forward direction). A

schematic layout of the experiments and typical spectra are shown in Fig. 17. The intent of these experiments was to show that the forward-scattered $3\omega_0/2$ spectra consist of only a single, blue-shifted component, as predicted by conventional theory for the scattering of incident photons from the higher-frequency plasmons produced by the TPD instability. In marked contrast to these predictions, our experiments on thin plastic foil showed forward-scattered $3\omega_0/2$ spectra consisting of a single, slightly red-shifted component (Fig. 17). Furthermore, the observed red-shift of the forward-scattered spectra was roughly equal to the shift of the blue component of the backscattered spectra at either 0° or 45° . The backscattered red component, in contrast, exhibited shifts which were two to three times larger. This asymmetry is, of course, exactly the same as that shown in Fig. 16 for thick targets, which could not be explained by conventional theory in Ref. 1. In the thin-target experiments, however, we noted a clear decrease of the intensity of the blue backscatter component relative to the red one.

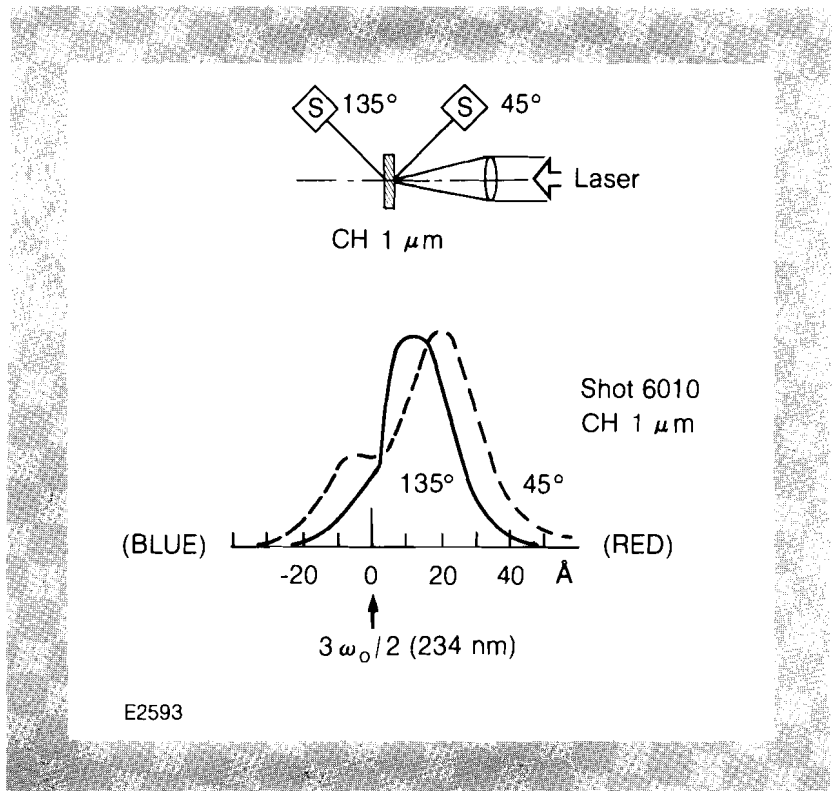
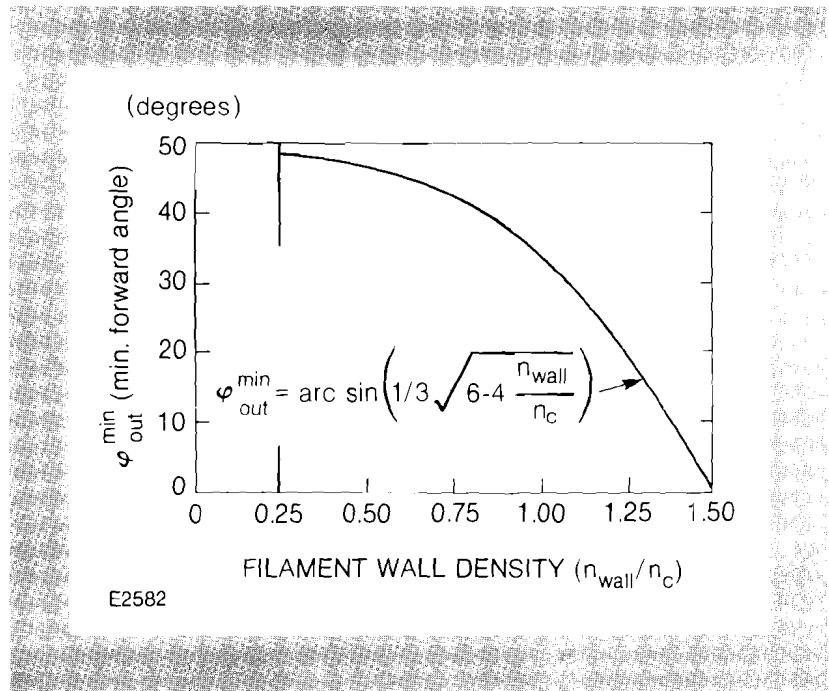


Fig. 17 Schematic of the experimental layout and typical $3\omega_0/2$ spectra observed in forward and backscattering from thin ($1\text{-}\mu\text{m}$ to $2\text{-}\mu\text{m}$) plastic targets irradiated at 10^{15} W/cm^2 at $\lambda_L = 351\text{ nm}$ and $t_L = 0.5\text{ ns}$. The slightly red-shifted, forward-scattered light is in accordance with the filamentation model.

This surprising experimental result finds a satisfactory answer in the framework of filamentation, as treated in the preceding article of this review. In this theory, a red forward-scattered $3\omega_0/2$ component was predicted if the angle of observation was not too close to the forward direction. In fact the cut-off angle for observing this component depends on the density of the background plasma through which the filament propagates and at which the TPD occurs inside the filament. Figure 18 is a rough estimate of this cut-off angle (ϕ) as a function of the background density. Ignoring non-planar-background plasma effects or distorted filament trajectories, we could use experimental

Fig. 18

Estimate of the minimum forward-scattering angle at which a red-shifted $3\omega_0/2$ component may be observed. The abscissa is the maximum background electron density through which the filament penetrated and at which the two-plasmon decay instability occurred inside the filament. The equation for ϕ_{out}^{min} contains phase-matching conditions for the $3\omega_0/2$ generation as well as refraction effects in the background plasma.

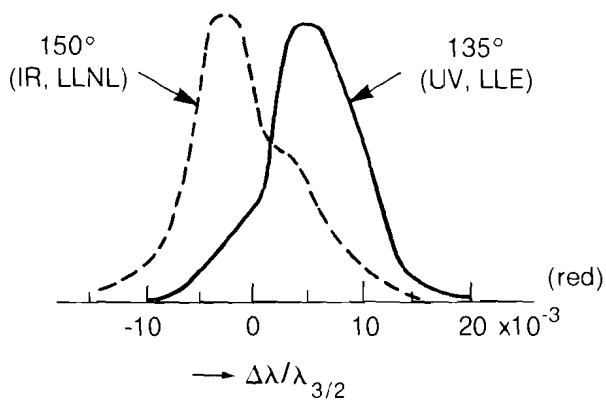


measurements of the cut-off angle as indication for the maximum background density through which the filaments penetrated. Conversely, observation of the change from red- to blue-shifted forward-scattered $3\omega_0/2$ radiation as a function of angle would constitute significant evidence for filamentation and the occurrence of TPD inside these filaments.

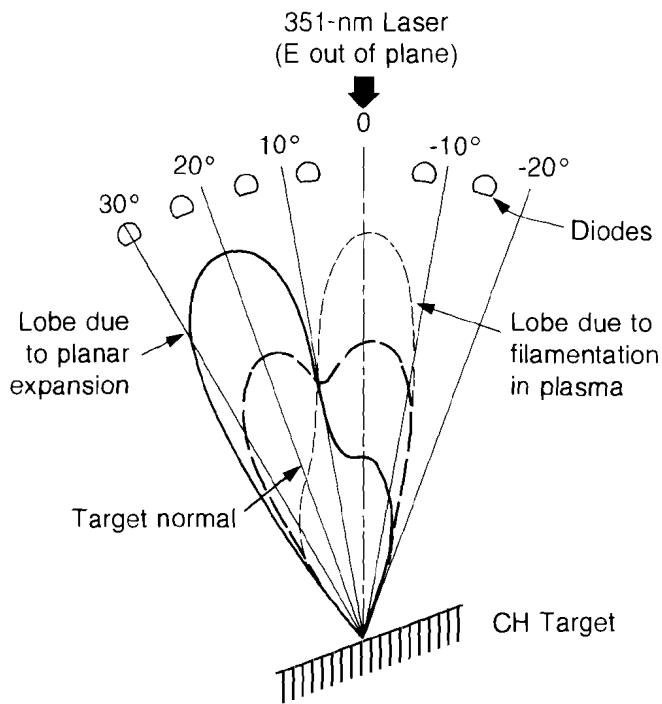
Although we have not yet investigated the $3\omega_0/2$ spectra in direct forward scattering there exists experimental data taken at 30° with respect to the forward direction from Shiva, planar, thin-foil IR irradiation experiments at the Lawrence Livermore National Laboratory.³ A scaled version of these data is shown in Fig. 19 along with one of our forward-scattering spectra observed at 45° to the forward direction. Although the experimental conditions were far from identical, we note that the Shiva data show approximately the same blue shift from the center ($3\omega_0/2$) frequency as the red shift for our data. This is predicted by the theory developed in the preceding article. Furthermore, the shifts for the red backscatter components are also in close agreement with the predictions.

Additional indirect evidence for the occurrence of TPD inside filaments has been observed in the angular distribution of the $\omega_0/2$ radiation emitted by our UV-laser plasmas. Figure 20 shows typical polar plots of this emission which usually consists of two lobes, one pointed along the target normal, the other one directed toward the incident laser (focusing lens). The former is the typical emission pattern expected for planar plasma blow-off in which all light generated at its own critical density is emitted normal to the target as a consequence of Snell's law. We propose that self-focusing of the laser light inside the plasma is responsible for the second component. Radiation at $\omega_0/2$ generated inside the filament and directed roughly

Fig. 19
 Spectra obtained for the $3\omega_0/2$, forward-scattered light at 135° (45° with respect to the forward direction) for the UV (LLE) data, and 150° (30° with respect to forward direction) for the IR (LLNL) data. From our analysis we conclude that ϕ_{out}^{min} for the observation of red, forward-scattered $3\omega_0/2$ radiation lies below 45° for the UV data and above 30° for the IR data.



E2583



E1897

Fig. 20
 Angular distribution of the scattered $\omega_0/2$ radiation from UV-laser plasmas. We note two lobes, one corresponding to the expected planar plasma blow-off, the other one due to filamentation of the incident laser light inside the plasma corona.

along the filament axis could then be guided out of the plasma without effectively seeing the overall planar-target plasma expansion. In general, we have observed that this emission pattern has a stronger self-focusing lobe for longer irradiation pulses as indicated in Fig. 20.

In short, we have presented experimental $3\omega_0/2$ -harmonic spectra from planar, single-beam, UV-laser plasmas which are well explained by the predictions, based on the TPD instability, made in the preceding article of this review. Since these experimental measurements cannot be explained on the basis of conventional planar-plasma blow-off, we believe that our data strongly suggest that TPD occurs, perhaps predominantly, inside filaments formed by the incident laser. Additional evidence has been found in the angular emission pattern of the $\omega_0/2$ radiation emitted from the same plasmas.

REFERENCES

1. LLE Review 14.
2. O. Willi, P. T. Rumsby, and Z. Kiu, Sixth Workshop on Laser Interaction with Plasma, Monterey, CA, 1982.
3. R. E. Turner *et al.*, Lawrence Livermore National Laboratory Report UCRL-86420, 1981.

Section 3

X-RAY LASER EXPERIMENTS

The extension of the laser into the x-ray range has long been the tantalizing objective of many research efforts. During the last twenty years, numerous papers have been published on a large variety of potential pumping schemes.¹ The enthusiasm for these studies has waxed and waned over this time, and although there have been overly optimistic claims which have not withstood the test of independent replication and close scrutiny, the objective has remained as unattainable as ever. The most publicized attempts to date, and those that have received the most attention, have been those x-ray laser schemes which employ high-power lasers to produce dense plasmas of highly stripped ions, in a geometric configuration designed to allow temporary population inversion to occur in the recombining plasma. Population inversion has been observed in recombining C, O, and Al plasmas.²⁻⁴ The latter work, performed with the GDL laser system at the University of Rochester with both circular and line focus conditions, used targets in which the plasma was cooled by the interjection of a secondary metal foil in close proximity to the laser plasma. Studies of this approach continue.

Since the summer of 1982, preparations have been under way at both LLE and LLNL to investigate another approach to x-ray lasers. The basis of this approach is the use of x rays from a laser-produced plasma to pump specific transitions in a gaseous plasma or medium. This approach has been considered by a number of workers in the past, but has, up to the present, undergone little experimental

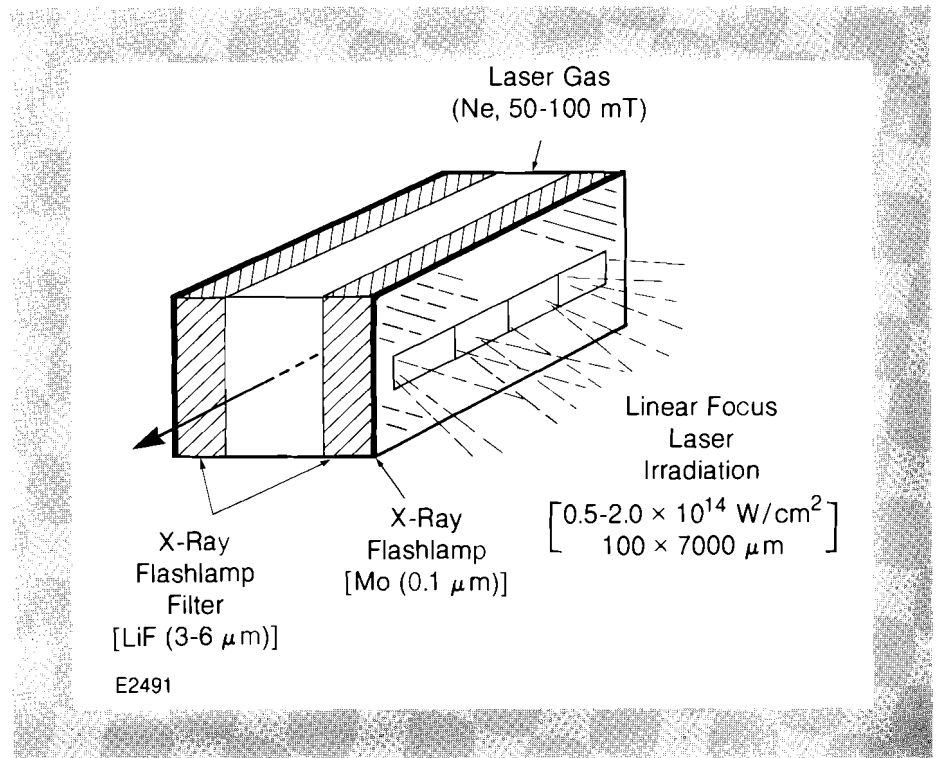
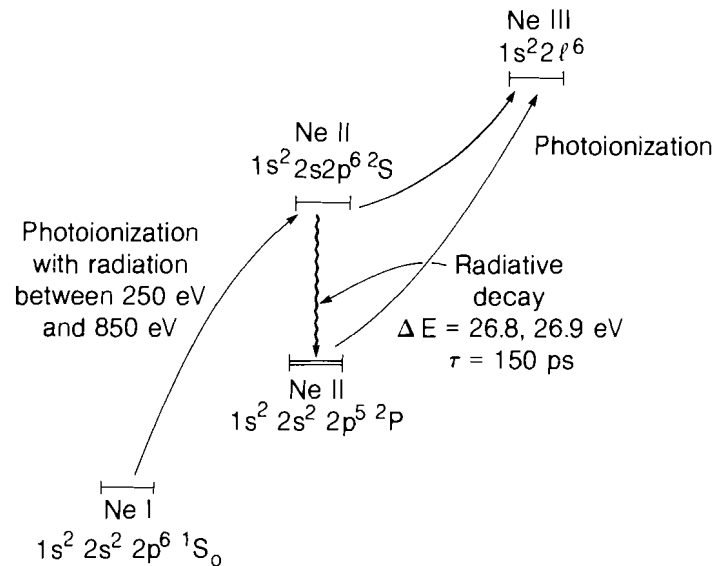


Fig. 21
Schematic of target configuration for laser-
pumped, photo-absorption x-ray laser.

investigation.⁵ Complex computations of this approach, using detailed hydrodynamic and atomic physics codes, have recently been made by Hagelstein.⁶

The general configuration of these types of x-ray laser experiments is indicated by the illustration in Fig. 21. A simple type of target consists of a rectangular gas-cell clad, preferably on both sides, with an x-ray filter and flashlamp assembly, the latter being irradiated by the laser beam or beams in line focus configuration. The close proximity of the flashlamp ensures good geometric coupling of the resulting x-ray emission to the laser medium; the thin x-ray filter prevents harmful spectral components of the flashlamp emission from detrimentally pumping the laser medium. The subsequent production of a transient population inversion in the gaseous or plasma medium may permit amplified spontaneous emission to be generated along the axis of the rectangular cell of the laser medium.

In this generalized approach to the application of laser-produced x rays to pump x-ray laser media, the emphasis has been on two specific schemes. In the first, x-ray line emission from specific transitions of highly ionized states in the x-ray flashlamp pump transitions in the x-ray laser medium. This approach can potentially demonstrate high gain for relatively high x-ray laser energies (i.e., short wavelengths), but does require exceedingly high tolerances in the degree of spectral overlap between the pumping radiation and the transition to be inverted. Investigations of this scheme are currently under way at Lawrence Livermore National Laboratory utilizing the new two-beam laser system, NOVETTE.⁷ NOVETTE is capable of producing $\sim 10^{14} \text{ W/cm}^2$ in line foci having dimensions of $100 \times 20,000$ microns.



E2492

Fig. 22
NeII photoionization-pumped lasing scheme (from Ref. 6).

The second scheme employs a different pumping scheme in which broadband x-ray emission in the range 300-800 eV photoionizes a cool gaseous medium. An example of this pumping scheme is illustrated in Fig. 22. In this particular case, rapid photoionization of NeI to NeII is created, such that there is a transient population inversion between the 2p and 2s states of NeII. From previous experimental measurements (Wuillermier⁸), it is known that the photoionization cross section for the 2p level is greater than that for the 2s level for x-ray emission in the 300-800 eV range. Although this approach does not depend on precise spectral overlap between the x-ray pump radiation and the medium to be pumped, it does require that the x-ray medium remain un-ionized prior to photoionization by the soft x-ray emission. Well-controlled focus conditions are required to ensure that the x-ray medium is not subject to electron or x-ray preheat prior to irradiation by the soft x-ray source. The magnitude of the population inversion is predicted to be critically dependent upon rapid photoionization of the two states; therefore ultra-short pulse irradiation of the laser flashlamps is required. Experiments designed to investigate this approach are currently being conducted on the OMEGA facility. Eight beams of OMEGA, those in clusters 5 and 2, were converted to line focus conditions, each beam providing a line focus of 1.6 mm in length and 100 μm in width at 1054-nm wavelength. Four beams from each cluster are aligned end-on to provide a total irradiated focal area of 100 μm by 7000 μm (Fig. 23). These experiments require the shortest pulses which OMEGA can safely provide. The OMEGA system is operating with 50-ps (FWHM) pulses and an energy of 20 J per beam;

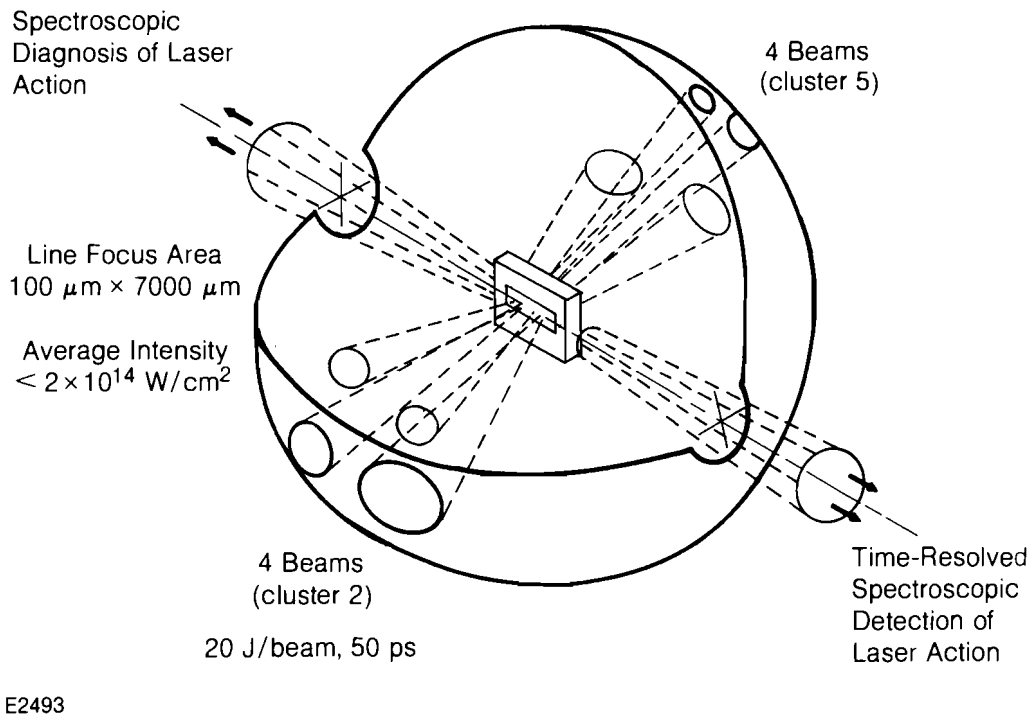


Fig. 23
Line-focus irradiation geometry on
OMEGA.

thus, an average intensity in the line focus of $\sim 2 \times 10^{14} \text{ W/cm}^2$ is produced. Significant new problems of alignment are created in these types of experiments. The eight individual line-focused beams must be aligned in the correct position relative to one another, on a common axis. In addition, this axis must also be colinear with the axis of the target and the axes of the various diagnostics used to analyze the output of the target. For the current experiments, the individual beams have to be positioned to an accuracy of approximately $50 \mu\text{m}$ on the target axis, which itself has been aligned to within 10^{-2} rad of the XUV spectrometers deployed to analyze the output of the target.

The x-ray laser experiments on OMEGA are composed of three distinct parts. Initially we performed test experiments in order to (a) determine the quality of the line focus, (b) activate a large number of new diagnostics, and (c) perfect methods for target and beam alignment. Figure 24 shows an x-ray pinhole camera image of the four-beam line focus demonstrating the degree of alignment and focusing of the individual beams. Figure 25 shows a high-resolution optical image of the $2\omega_0$ emission from the focal region of the overlap of two beams. Microscopic structure emanating away from the focal region is clearly visible; this is suggestive of the existence of microscopic plasma or filamentary structures.

This phase of the program was followed by a short series of experiments to analyze the x-ray performance of the x-ray flashlamp

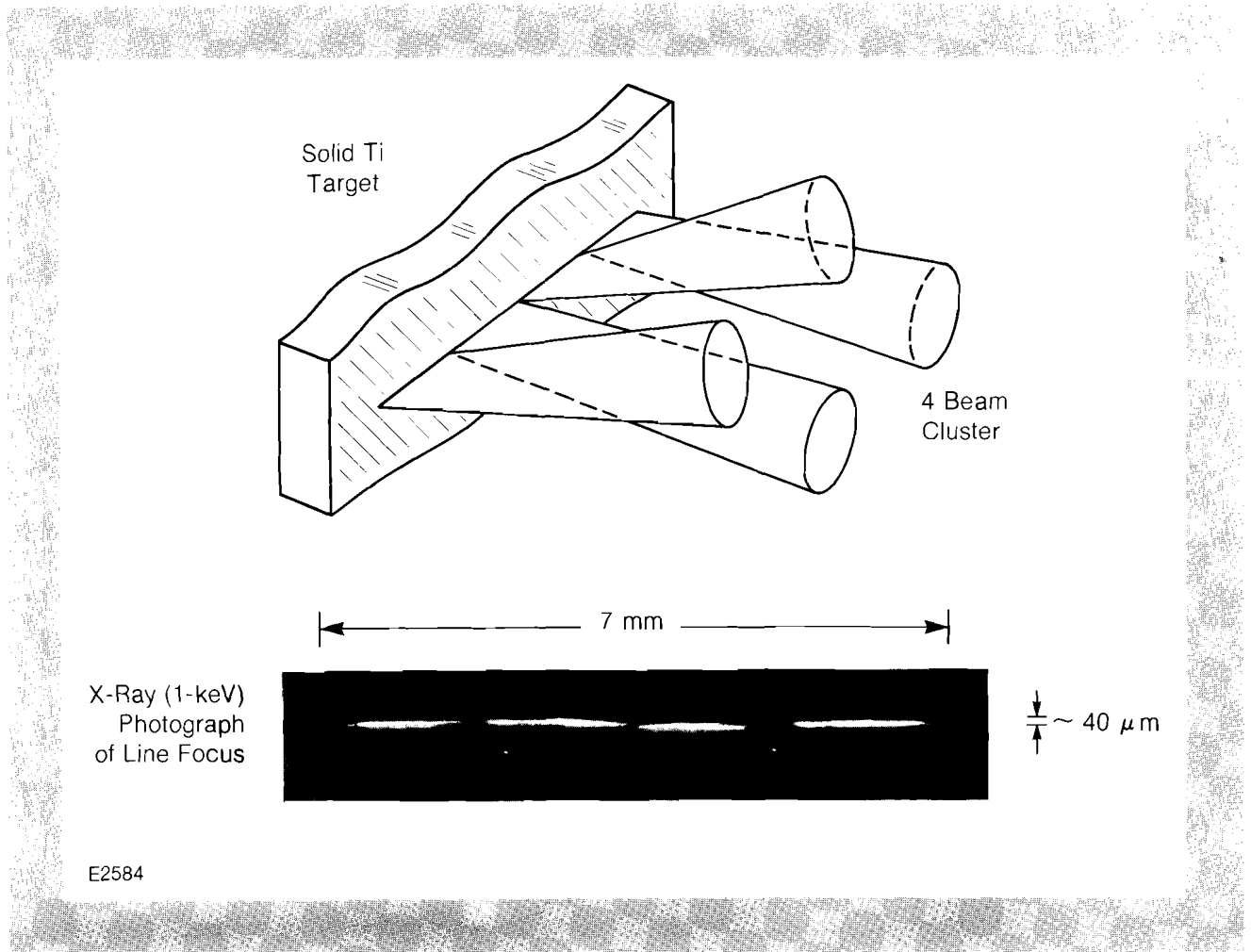


Fig. 24
X-ray pinhole camera image of four-beam
line focus on OMEGA.

and filter assemblies. Finally, a series of experiments was performed on integral gas-filled targets, to examine the performance and potential of this approach to x-ray lasers. Detailed results from these experiments will be presented and analyzed in a future issue of LLE Review.

REFERENCES

1. Reviews of x-ray laser studies can be found in R. W. Waynant and R. C. Elton, *Proc. IEEE* **64**, 1059 (1976) and G. Chapline and L. Wood, *Phys. Today* **28**, 40 (1975).
2. R. J. Dewhurst, D. Jacoby, G. J. Perk, and S. A. Ramsden, *Phys. Rev. Lett.* **37**, 1265 (1976).
3. T. C. Bristow, M. J. Lubin, J. M. Forsyth, E. B. Goldman, and J. M. Soures, *Opt. Commun.* **5**, 315 (1972).
4. V. A. Bhagavatula and B. Yaakobi, *Opt. Commun.* **24**, 331 (1978); Y. Conturie, B. Yaakobi, J. Delettrez, and J. M. Forsyth, *Laser Techniques for Extreme Ultraviolet Spectroscopy*, AIP Conference Proc. No. 90., p. 312 (1982).
5. M. A. Duguay and P. M. Rentzipis, *Appl. Phys. Lett.* **10**, 350 (1967).

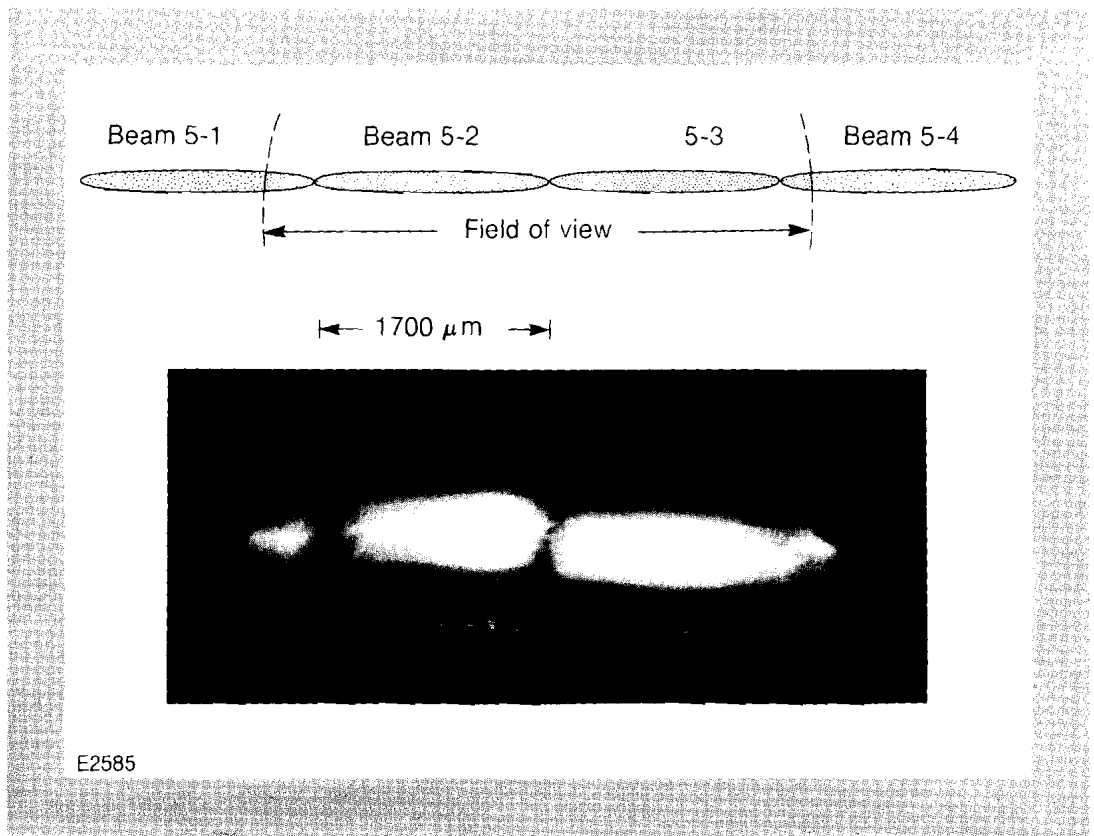


Fig. 25
Image of $2\omega_0$ emission from OMEGA line-focus experiment showing the region of overlap of two beams.

6. P. Hagelstein, Lawrence Livermore National Laboratory Report UCRL-53100 (1981).
7. D. L. Mathews *et al.*, Proc. 1983 CLEO Conference, p. 164 (1983).
8. F. Wuilleumier, *Adv. X-Ray Anal.* **16**, 63 (1973).

Section 4

ADVANCED TECHNOLOGY DEVELOPMENT

4.A Liquid-Crystal Laser-Blocking Filters

In various laser applications, situations often arise which require selective optical filtration. Optical elements which exhibit extremely low transmittance at the specific laser wavelength, λ_0 , and high transmittance at other wavelengths are required to filter optical radiation incident, for example, upon ultraviolet (UV) diagnostics or infrared (IR) thermal-imaging systems. Laser goggles for eye protection of personnel constitute another area where laser-blocking notch filters are useful. Figure 26 gives an example of spectral transmission characteristics of a generic notch filter.

Some of the design and performance goals for a laser-blocking notch filter operating at a wavelength of λ_0 are as follows:

- 1) attenuation at λ_0 greater than 10^3 ;
- 2) transmittance away from λ_0 better than 85%;
- 3) ease of alignment, or broad angular acceptance;
- 4) a device that is compact, lightweight and inexpensive; and
- 5) adequate laser-damage resistance.

High in-band attenuation and high out-of-band transmittance are required to provide optical sensors with protection against lasers without sacrificing the ability to detect background radiation. Angular insensitivity to laser radiation and light weight are important for personnel protection devices such as laser goggles.

Absorbing glasses or dye/plastic filters, thin-film interference filters,¹ and holographic filters² are examples of materials technologies that

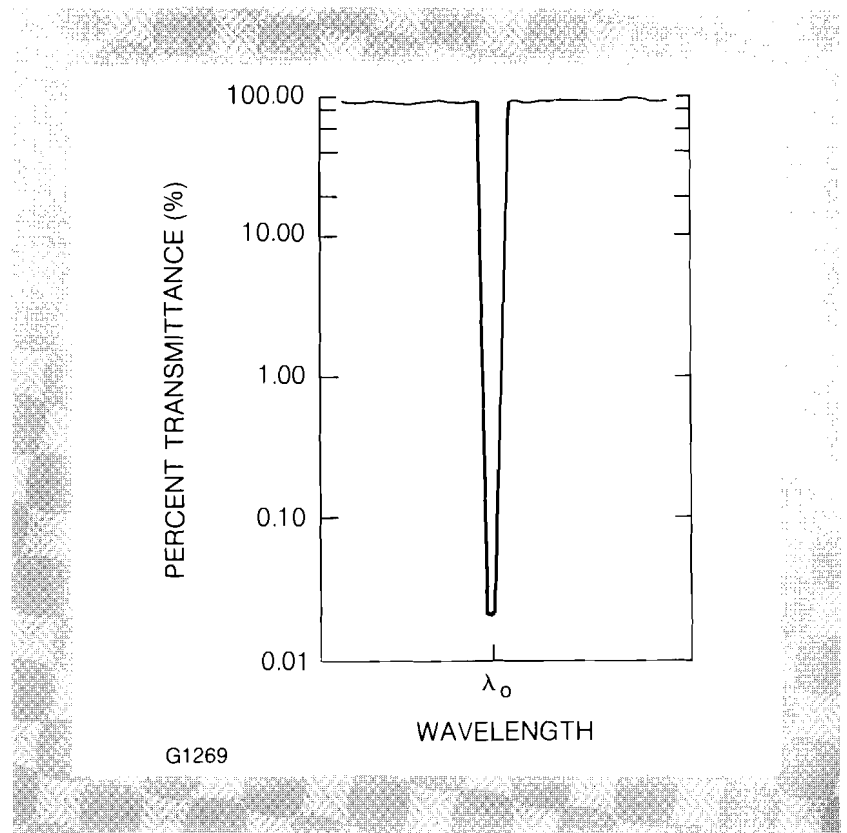


Fig. 26
Spectral characteristics of a laser-blocking notch filter. Laser radiation at $\lambda = \lambda_0$ is attenuated, whereas background optical radiation at shorter and/or longer wavelengths is transmitted with negligible loss.

have been used to construct notch filters. None of these approaches has succeeded in meeting all of the performance goals listed above. Liquid crystals offer an alternative method for constructing laser-blocking notch filters which approaches more closely the concept of a perfect notch filter.

The cholesteric class of liquid-crystal compounds exhibits the unusual property of selective reflection.³ (The reader is referred to the article on liquid crystals in Volume 5 of the LLE Review, and the figures therein, for a more complete discussion of the structure and properties of cholesteric liquid crystals.) The basis for this effect resides in the spontaneous, helical alignment exhibited by cholesteric molecules on a microscopic scale. Through the use of suitable preparation techniques to induce helical alignment over macroscopic distances, liquid-crystal cells can be fabricated which act as nearly perfect circular polarizers. Optical radiation incident upon a cell is totally reflected if its polarization sense matches the chirality, or helicity, of the cholesteric compound.⁴ (Unlike the case for standard reflection from a dielectric at near-normal incidence, the phase of the light reflected by the liquid-crystal cell is *not* shifted by 180°.) The orthogonal polarization is transmitted with negligible loss. The effect is strong, and a fluid layer no more than a few tens of microns in thickness is required. The wavelength selectivity of this effect arises because optical radiation interacts with the cholesteric structure only if the wavelength λ_0 satisfies the equation:

$$\lambda_0 = n_n p \quad (1)$$

where n_n is the average refractive index of the cholesteric, and p is a measure of the pitch of the molecular helix. The selective reflection effect may be shifted from the UV to the IR by creating an appropriate mixture of cholesteric compounds with different values of intrinsic pitch.

Notch filters may be constructed from cholesteric liquid crystals by stacking together two liquid-crystal cells filled with fluids possessing opposite chiralities, which have been tuned to the same wavelength, λ_0 .⁵ The concept is shown in Fig. 27. At the wavelength for selective reflection, the device performs as a nearly perfect pair of crossed circular polarizers, blocking incident laser radiation. Optical radiation at wavelengths away from λ_0 is transmitted through the filter with negligible attenuation.

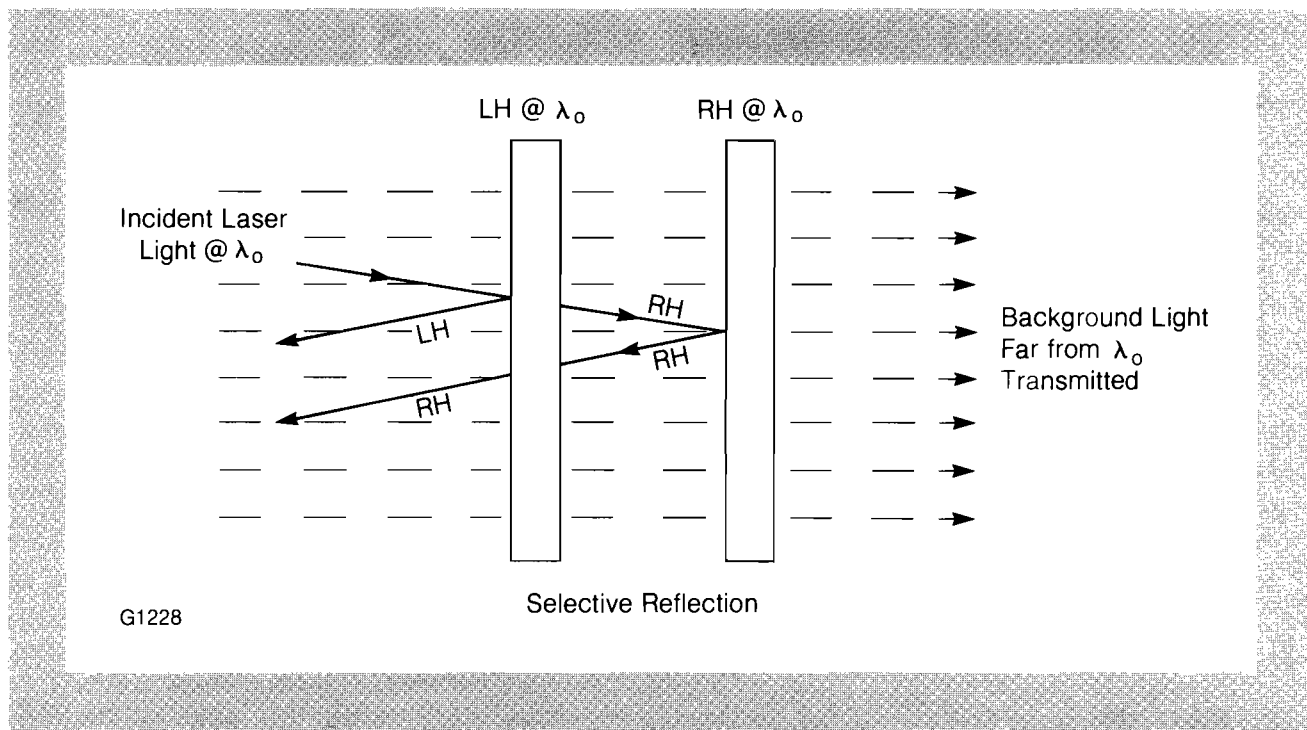


Fig. 27
Liquid-crystal laser-blocking filter concept. The filter consists of two liquid-crystal cells. Each cell is filled with a cholesteric compound tuned to exhibit selective reflection at the laser wavelength, λ_0 . Because the mixtures have opposite senses of helical alignment (one is left-handed whereas the other is right-handed), the device acts as a pair of crossed circular polarizers to block the transmission of laser radiation at λ_0 . Background optical radiation at $\lambda \neq \lambda_0$ is transmitted through the filter with negligible attenuation, due to the wavelength-selective nature of the effect.

We have constructed and characterized a number of liquid-crystal laser-blocking filters at LLE. The 38-mm-diameter substrate material for our experiments is fused silica. Liquid layer spacers are cut from "Mylar" films that vary in thickness from 6 to 36 μm . Cells are sealed with either quick-drying epoxy or UV-curing cement. Left-handed and right-handed mixtures of appropriate pitch are prepared from commercially available nematic and cholesteric compounds without additional purification. (Nematics may be thought of as liquid crystals with infinite pitch. Refer to Volume 6 of the LLE Review for a discussion of this class of liquid-crystal materials.) Table 1 lists some of these compounds, their helical sense, and the short-wavelength boundary (discussed below). All mixtures are chemically and photochemically stable, and are relatively insensitive to temperature.

TYPE	MATERIAL (source)	MESOPHASE RANGE, °C	Δn @ $\lambda = 589 \text{ nm}$	CHIRALITY (handed- ness)	SHORT WAVELENGTH LIMIT, nm (tight pitch constraint)
Nematic	ROTN-701 (HL ^a)	-10 to +60.5	0.150	∞	
	ZLI-1167 (EM ^b)	+32 to +83	0.060	∞	
	ZLI-1646 (EM)	-7 to +60	0.080	∞	
	S-1236 PCH (HL) NM-820303 (ALX ^d)	40 ^c	0.133	∞	
Cholesteric	CB-15 (EM)			RH	
	C-15 (EM)			LH	
	COC-Cholesteryl Oleyl Carbonate (EK ^e)			LH	
	CN-Cholesteryl Nonanoate (EK)			LH	
	CO-Cholesteryl Oleate (EK)			LH	
	CAA-Cholesteryl Amyl Alcohol (ALX) CEC-Cholesteryl Ethyl Carbonate (S ^f)			RH LH	
Commercial Mixtures	NM-109-15 (ALX)			LH	
	NM-021008 (ALX)			RH	
LLE Mixtures	NM109-15 + CN			LH	> 390
	NM109-15 + CEC			LH	> 390
	NM109-15 + COC			LH	> 385
	NM-021008 + CB-15			RH	> 400
	NM-021008 + CAA			RH	> 450
	NM-820303 + CO			LH	> 400
	XLI-1167 + CB-15			RH	> 385
	ROTN-701 + BA-15			RH	> 430

a Hoffman LaRoche, Nutley, New Jersey
 b EM Chemicals, Hawthorne, New York
 c preserves nematic order upon cooling to 4°C
 d American Liquid Xtal Chemical Corp., Kent, Ohio
 e Eastman Kodak Company, Rochester, New York
 f Sigma Chemical Co., St. Louis, Missouri

G1270

Table 1 Liquid-crystal materials for notch-filter fabrication.

Cary 14 spectrophotometer scans of notch filters fabricated for several laser wavelengths are shown in Fig. 28. Blocking ratio measurements performed on these cells using laser ratiometry with lock-in detection indicate that extinctions in excess of 10^3 can be achieved in the visible and near-infrared regions for fluid layers $11 \mu\text{m}$ thick. The width of the selective reflection peak is given as

$$\Delta\lambda_{\text{FWHM}} = \frac{\Delta n_n}{n_n} \lambda_o \quad (2)$$

where Δn_n is the optical birefringence of the mixture. The notch-filter bandwidth may be adjusted from approximately 20 nm to 120 nm in the visible and near-infrared regions by choosing liquid-crystal compounds which maximize or minimize the optical birefringence.

The angular sensitivity of the selective reflection effect may be calculated from the formula⁶

$$\lambda = \lambda_o \left[\sin^{-1} \left(\frac{1}{n_n} \sin\theta \right) \right] \quad (3)$$

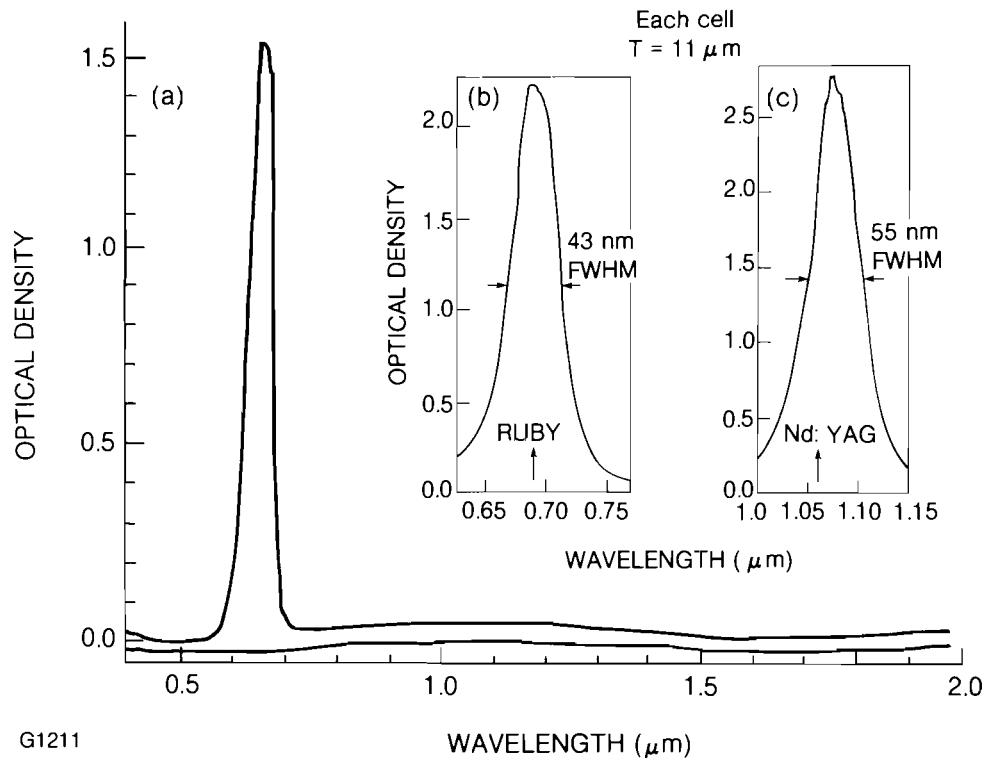
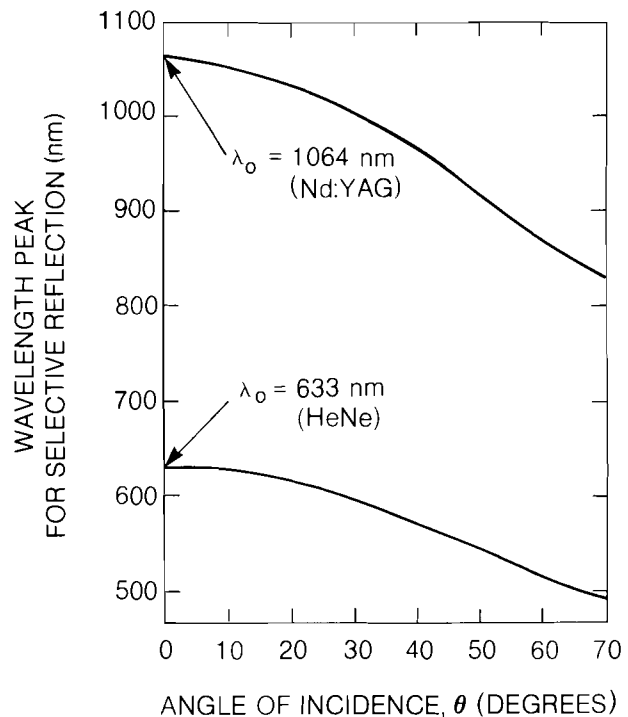


Fig. 28

Cary 14 spectrophotometer scans of notch filters. Each filter is composed of two cells whose fluid-layer thickness is $11 \mu\text{m}$. Composition tuning of λ_0 allows the peak for selective reflection to be adjusted to (a) doubled Nd:YAG at 532 nm, (b) ruby at 694 nm, and (c) Nd:YAG at 1064 nm.

In this formula it is assumed that the angles of incidence and observation, θ , are equal. Figure 29 demonstrates how the selective-reflection wavelength peak shifts as a function of θ according to Eq. 3. The tendency for the peak-to-shift toward shorter wavelengths as θ increases may be incorporated into the design of notch filters to reduce their angular sensitivity further. Filters may be fabricated with λ_0 peaks at normal incidence which are several percent longer than the laser wavelength being blocked. As is demonstrated in Fig. 30, the non-normal incidence blocking capability for these detuned filters is enhanced over that of tuned filters without a significant degradation in normal incidence performance. An increased acceptance angle of $\pm 15^\circ$ at a blocking extinction ratio of 10^3 has been demonstrated.

We are currently determining the factors which limit the use of liquid crystals as notch filters over the optical spectrum. The major impediment to notch-filter construction in the UV appears to be our inability to induce a sufficiently tight (or short) pitch by using the compounds listed in Table 1 to shift λ_0 to wavelengths below 385 nm. Optical absorption does not become a problem for the most transmissive materials until a wavelength of 310 nm is approached. Average internal transmittance in the infrared between 2.5 and $5 \mu\text{m}$ for cells $50 \mu\text{m}$ thick is better than 90% for phenylcyclohexane compounds; the transmittance approaches 80% for the cyanobiphenyl K-15 in the thermal-imaging band between 8 and $12 \mu\text{m}$.⁷ Useful trans-



G1271

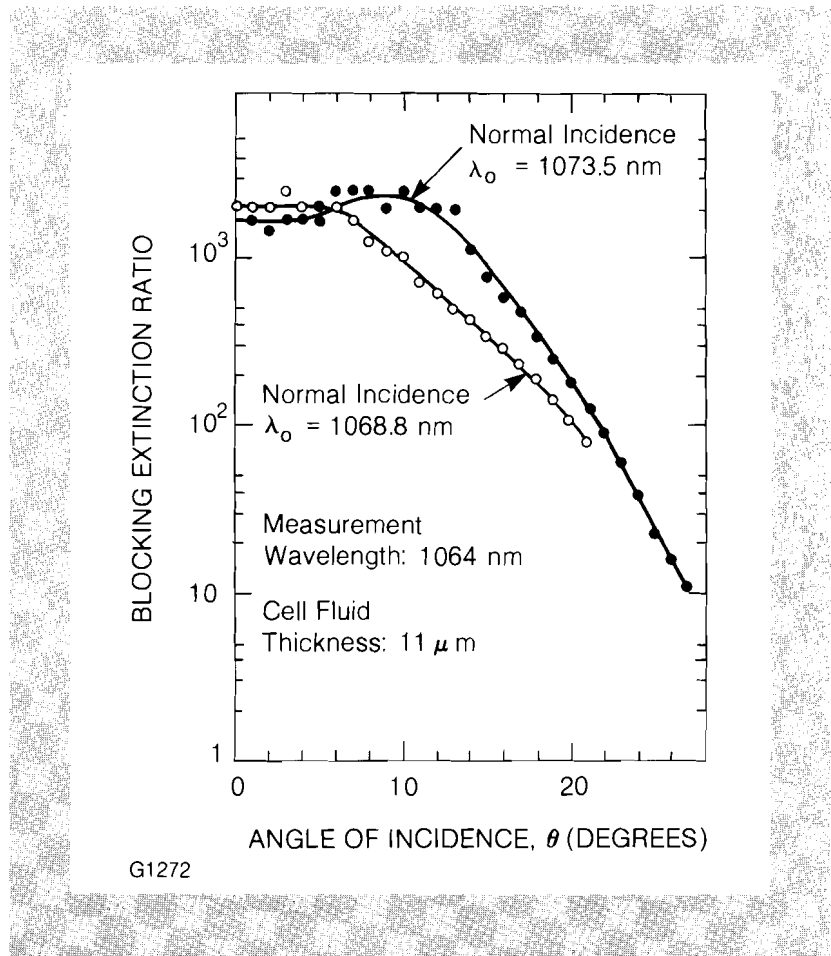
Fig. 29

Shift in selective-reflection peaks versus angle of incidence. The curves are calculated from Eq. 3 for single cells tuned to $\lambda_0 = 1064$ nm and $\lambda_0 = 633$ nm at normal incidence.

mission in the infrared extends beyond $16 \mu\text{m}$. The laser-damage threshold of these compounds is of the order of $20 \text{ GW}/\text{cm}^2$ (50 ps, $\lambda = 1054$ nm) or $2 \text{ J}/\text{cm}^2$ (750 ps, $\lambda = 1054$ nm). It is therefore possible to consider liquid-crystal notch filters for use in blocking most gas and solid-state lasers operating from the ultraviolet through the infrared region.

REFERENCES

1. M. Speciale and F. Zmarzly, *Military Electronics/Countermeasures*, p. 43 (February 1983).
2. D. J. Coleman and J. R. Magarinos, *J. Opt. Soc. Am.* **72**, 1831 (1982).
3. J. L. Ferguson, *Sci. Am.* **211** (2), 77 (1964).
4. D. M. Makow, *Color Research and Applications* **4**, 25 (1979).
5. J. Adams, W. Haas, and J. Dailey, *J. Appl. Phys.* **42**, 4096 (1971).
6. J. L. Ferguson, in *Liquid Crystals*, edited by Brown, Dienes, and Labes (Gordon and Breach, New York, 1965) p. 89.
7. J. G. Pasko, J. Tracy, and W. Elser, "Active Optical Devices," *SPIE Vol. 202*, 82 (1979).



4.B Sub-Micron X-Ray Lithography Using UV-Laser-Produced Plasma as a Source

The production of integrated circuits in the computer and electronic industries is currently done by photolithography. In the future, more powerful circuits will have to contain smaller circuit elements. Photolithography will not be effective in producing elements smaller than $\sim 1 \mu\text{m}$, because light diffraction causes loss of resolution. Instead, the most probable solution would be to (a) fabricate masks with an electron beam, and then to (b) mass-replicate these masks with x rays.

X-ray lithography has been used successfully over the last few years to produce relief structures of submicron dimensions. The commercial application of x-ray lithography to the production of integrated circuits will depend on progress in a few interrelated areas: the resist, the mask, the relative placement and alignment of mask and resist, and the x-ray source. Any development in any one area may change the design philosophy and optimal parameters considerably.

The plasma produced by focusing a laser onto a target is an intense x-ray source of very small dimensions, which makes it very well suited for high-resolution lithography. In addition, our x-ray lithographic experiments show that a modest pulse energy (35 J) is sufficient for pattern registration in PBS and other resists at a distance of 10 cm from the laser target. These characteristics make laser plasma a promising source for commercial x-ray lithography.

X-ray lithography using laser-produced plasma as a source has been reported in the past. In one such study,¹ 40-ns, 100-J pulses of a wavelength of 1060 nm were used. As many as 60 to 90 laser shots had to be integrated over, in order to obtain PBS exposure at a distance of 5 cm from the target. Using the GDL laser system in the configuration shown in Fig. 31, we find here that a single, $\lambda = 351$ nm, 1-ns laser shot of energy 35 J, is sufficient to produce submicron patterns in PBS at a distance of 10 cm from the target. This improved performance can be attributed to two factors:

- a) By using a UV ($\lambda = 351$ nm) rather than an IR laser, the x-ray production efficiency for given focusing conditions is greatly improved.² This also means a concomitant reduction in the remainder of the absorbed energy which appears as kinetic energy of the target debris. Hence, the damage to the mask for a given x-ray flux is reduced, permitting the use of a thinner, more transmissive filter for protecting the mask. Even though we lose intensity when frequency-tripling the IR laser (the conversion efficiency³ actually exceeds 50%), this is more than compensated by the higher efficiency of x-ray production.
- b) We find that the x-ray flux sufficient to produce resist exposure is lower than that predicted by published sensitivity data for the same resist and processing conditions. We tentatively attribute this to some combination of two factors: the short (~ 1 -ns) duration of the exposure pulse, and an abrupt rise in the temperature of the resist due to heat generated when the target debris strike the filter which is used to protect the mask.

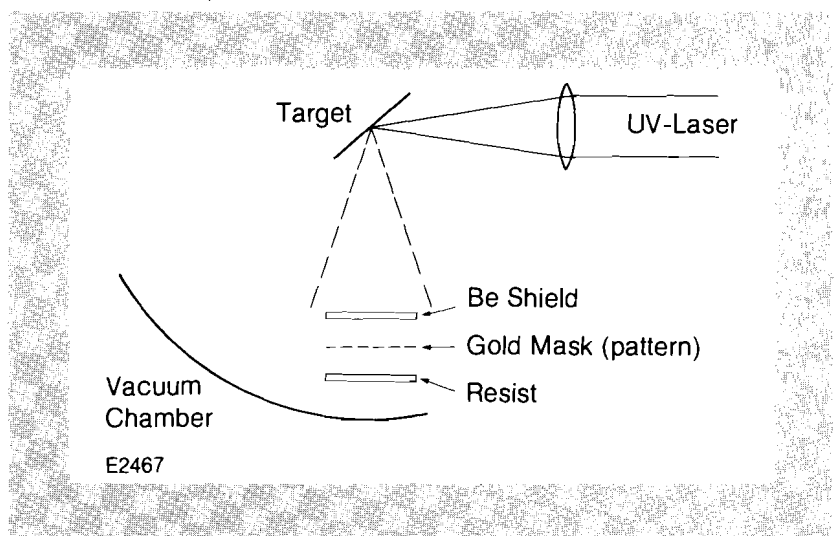


Fig. 31
Geometry for x-ray lithography using laser-produced plasma as a source. The shield protects the mask and resist from the impact of target debris.

In order to determine the resist sensitivity in our exposure system, we have to sum up contributions of the various energy groups comprising the emitted x-ray spectrum. The spectrum emitted by an iron target is shown in Fig. 32. It comprises a K-shell emission feature near 8 keV (unresolved lines of Fe^{24}) as well as a broad continuum. Integrating over the spectrum and angles (using a measured angular distribution²), we find 5.7 J of x rays emitted, or 27% of the laser energy absorbed in the target.

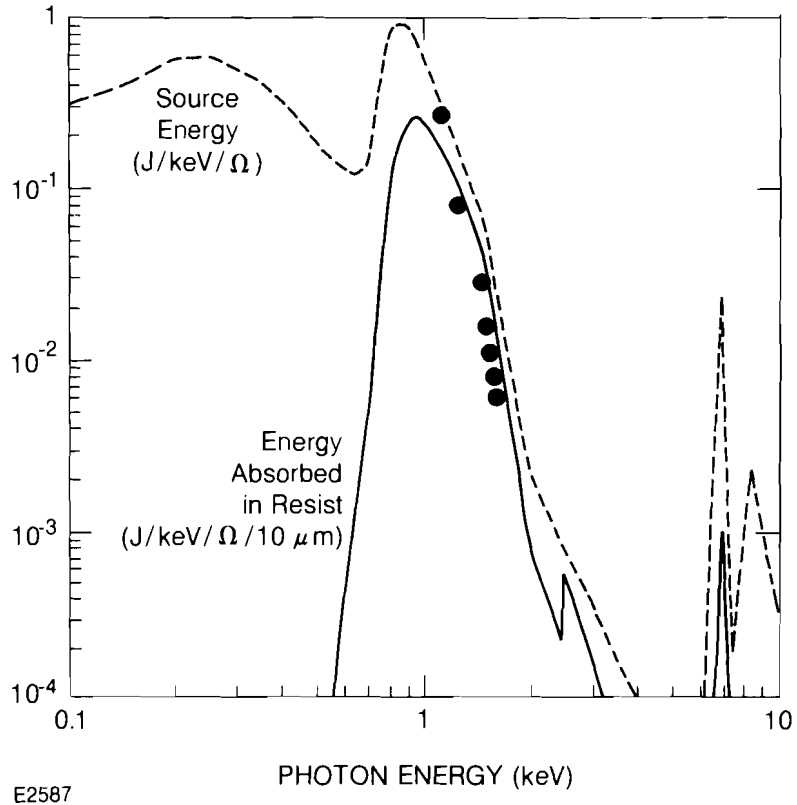


Fig.32

X-ray spectrum emitted by an iron target irradiated by a 1-ns, 351-nm laser pulse of energy 35 J. The solid curve is obtained from the emitted spectrum after multiplying by the beryllium window transmission and the resist (PBS) absorption coefficient. The circles and the spectral features above 7 keV represent measurements; the emitted continuum is from numerical simulation.

We next calculate the spectrum transmitted through the 18- μm -thick beryllium filter. This has the effect of essentially removing the subkilovolt part of the spectrum while leaving the intensity above ~ 1 keV almost unaffected. The energy absorbed per unit depth at the surface of the resist is obtained by multiplying the incident x-ray intensity by the linear absorption coefficient. The result is shown by the solid line in Fig. 32.

The total x-ray energy transmitted through a beryllium filter is 0.72 J. The x-ray-energy-density incident on the resist, located 10 cm from the target is 0.57 mJ/cm². Finally, the total x-ray energy per unit volume absorbed at the surface of the resist is 0.9 J/cm³. The sensitivity expressed as energy absorbed per unit volume is essentially independent of wavelength,⁴ and can be directly compared with

published data. The published sensitivity data for PBS,^{5,6} processed in the same way as here, is 14 J/cm^2 . Our exposure system appears, therefore, to be more sensitive by about one order of magnitude than the results of published PBS sensitivity data.

We show in Fig. 33 examples of imprinted mask patterns in PBS resists using as a mask an unsupported gold grating of $0.45\text{-}\mu\text{m}$ linewidth.

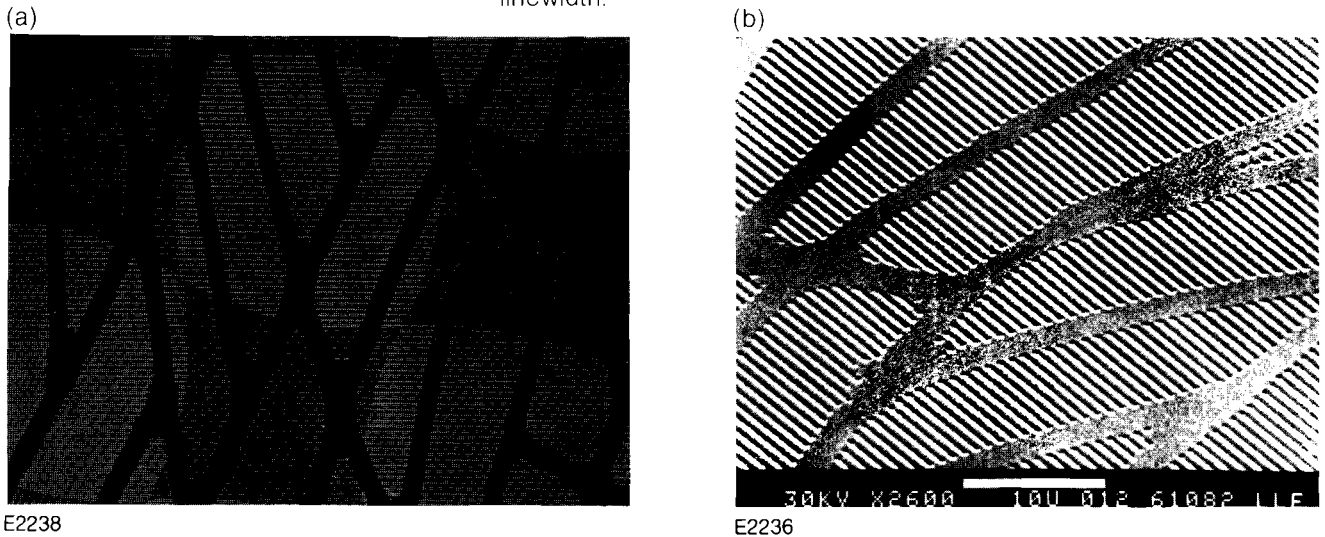


Fig. 33
Examples of PBS resist registration through a $0.45\text{-}\mu\text{m}$ -linewidth gold grating. The coarse struts (of gold) serve as a support structure but the mask is free-standing (unbacked). A single, 35-J pulse of UV laser was used.

- a) Phase-contrast optical microscope image of imprinted image.
- b) Scanning electron-microscope image of imprinted image.

In summary, the favorable exposure characteristics found here, in addition to the more obvious relative advantages, make the laser-produced x-ray source promising for sub-micron lithography. Some of these advantages over other x-ray sources are: (a) small dimensions ($< 0.1 \text{ mm}$), (b) reproducibility of source positioning (to a few μm), (c) almost complete freedom in choosing the target material (which affects the spectral characteristics), and (d) mechanical stability in single-pulse operation.

REFERENCES

1. D. J. Nagel, M. C. Peckerar, R. R. Whitlock, J. R. Grieg, and R. E. Pechacek, *Electron. Lett.* **14**, 781 (1978).
2. W. C. Mead, E. M. Campbell, K. G. Estabrook, R. E. Turner, W. L. Kruer, P. H. Y. Lee, B. Pruett, V. C. Rupert, K. G. Tirsell, G. L. Stradling, F. Ze, C. E. Max, and M. D. Rosen, *Phys. Rev. Lett.* **47**, 1289 (1981).
3. W. Seka, S. D. Jacobs, J. E. Rizzo, R. Boni, and R. S. Craxton, *Opt. Commun.* **34**, 469 (1980).
4. E. Spiller and R. Feder, in *X-Ray Optics*, edited by H. J. Queisser (Springer-Verlag, Berlin, 1977), p. 49, also p. 54.
5. L. F. Thompson, E. D. Feit, M. J. Bowden, P. V. Lenzo, and E. G. Spencer, *J. Electrochem. Soc.* **121**, 1500 (1974).
6. P. V. Lenzo and E. G. Spencer, *App. Phys. Lett.* **24**, 289 (1974).

Section 5

NATIONAL LASER USERS FACILITY NEWS

This report covers the activities of the National Laser Users Facility (NLUF) during the quarter April to June 1983. During this period, three users conducted experiments on LLE facilities. The visiting scientists associated with these experiments represented the University of Pennsylvania, the University of Connecticut, and the Naval Research Laboratory and are listed below:

1. J. K. Blaise, D. Pierce, D. Pascolini, and A. Scarpa (University of Pennsylvania).
2. L. Herbette and R. McDaniel (University of Connecticut).
3. R. Elton and T. N. Lee (Naval Research Laboratory).

During this quarter, on May 13, 1983, the NLUF Steering Committee held its fourth meeting to review and approve proposals, and to recommend funding of approved proposals in inertial fusion to the Department of Energy. This funding allocation is separate from LLE's operation contract, and is designed to provide research funds to users in the inertial fusion field. Users in other fields may use the facility but must provide their own research funds.

The Steering Committee membership changed somewhat from the previous meeting as several new people were invited to serve on the committee. We expect this rotation to continue for future meetings. The scientists participating as Steering Committee members represented a broad range of research areas including laser fusion,

astrophysics, biophysics, optics, nuclear physics, and magnetic fusion. The committee membership consisted of:

- Brian J. Thompson**, Chairman
(Dean, College of Engineering, University of Rochester)
- Thomas C. Bristow**, non-voting Executive Secretary
(NLUF Manager)
- David T. Attwood**
(Laser Program, Lawrence Livermore National Laboratory)
- John C. Browne**
(Los Alamos National Laboratory)
- Donald L. D. Caspar**
(Rosenstiel Research Center, Brandeis University)
- Gordon P. Garmire**
(Department of Astronomy, Pennsylvania State University)
- Wulf B. Kunkel**
(Department of Physics, University of California at Berkeley)
- Barry H. Ripin**
(Naval Research Laboratory)
- Donald C. Slater**
(KMS Fusion, Inc.)

The committee approved 11 of the 22 proposals. The approved experiments are in the areas of plasma physics, laser fusion, and x-ray biophysics. The new approved proposals are:

1. **Prof. J. Kent Blasie** (University of Pennsylvania): "A Continuation Proposal for Time-Resolved Structural Studies of the Ca²⁺-ATPase of Sarcoplasmic Reticulum Membranes Utilizing a Laser-Plasma X-Ray Source."
2. **Dr. Phillip G. Burkhalter** (Naval Research Laboratory): "X-Ray Spectroscopy to Determine Line Coincidences Between K- and M-Series Transitions."
3. **Prof. Carl B. Collins** (University of Texas at Dallas): "The Study of Nuclear Fluorescence Excited by Laser-Plasma X Rays."
4. **Dr. Raymond C. Elton** (Naval Research Laboratory): "Pumping of a Soft X-Ray Laser as a High-Density Plasma Probe."
5. **Dr. Uri Feldman** (Naval Research Laboratory): "A Proposal for the Measurement of the Spectra of Neon-Like Ions Relevant to X-Ray Lasers Using the OMEGA Laser Facility."
6. **Prof. Hans R. Griem** (University of Maryland): "Shifts and Widths of Hydrogenic Ion Lines: Experimental Proposal for Continuation of Measurements at the University of Rochester Laser Users Facility."

7. **Dr. Allan Hauer** (Los Alamos National Laboratory): "Diagnosis of High-Density Laser-Driven Compressions with Novel X-Ray Spectroscopic Techniques."
8. **Prof. Burton L. Henke** (University of Hawaii at Manoa): "Evaluation and Application of a Streak Camera and Photographic Camera Coupled Elliptical-Analyzer Spectrograph System for the Diagnosis of Laser-Produced X-Ray Sources (100-10,000 eV Region)."
9. **Prof. Leo G. Herbette** (University of Connecticut Health Center): "Time-Resolved X-Ray Diffraction of Acetylcholine Receptor Membranes."
10. **Prof. Chan Joshi** (UCLA) and **Prof. Nizarali A. Ebrahim** (Yale University): "Studies of the Two-Plasmon Decay and Stimulated Raman Scattering Instabilities in Hot, Long-Scale-length Plasmas."
11. **Prof. Benjamin Post** (Polytechnic Institute of New York): "X-Ray Crystal Devices for Measuring Compression and Stability of Laser-Fusion Targets."

Further information on the NLUF is available by writing to:

Thomas C. Bristow, Manager
National Laser Users Facility
Laboratory for Laser Energetics
250 East River Road
Rochester, New York 14623

PUBLICATIONS AND CONFERENCE PRESENTATIONS

Publications

M. C. Lee, I. Feng, T. G. Wang, and H. Kim, "A Technique for Thick Polymer Coating of Inertial-Confinement-Fusion Targets," *J. Vac. Sci. Technol.* **1**, 886-889 (1983).

B. A. Brinker, J. M. Cavese, J. R. Miller, S. G. Noyes, S. Sheble, and L. T. Whitaker, "Inertial Fusion Target Mounting Methods: New Fabrication Procedures Reduce the Mounting Support Perturbation," *J. Vac. Sci. Technol.* **1**, 941-944 (1983).

D. Glocker, "Biased Magnetron Sputtering of ICF Target Pusher Layers," *J. Vac. Sci. Technol.* **1**, 877-880 (1983).

H. Kim, J. Mason, and J. R. Miller, "High-Z-Doped Laser Fusion Target Ablation Layers Using Metal Colloids and Metal-Substituted-Sulfonated Polystyrene," *J. Vac. Sci. Technol.* **1**, 890-893 (1983).

T. F. Powers and J. R. Miller, "Rotational-Shearing Interferometric Characterization of Inertial Fusion Targets," *J. Vac. Sci. Technol.* **1**, 945-948 (1983).

J. Reynolds, "Information Management Data Base for Fusion Target Fabrication Processes," *J. Vac. Sci. Technol.* **1**, 937-940 (1983).

S. Sarraf and E. A. Williams, "Ion-Ion Two-Stream Instability in Multispecies Laser-Produced Plasma," *Phys. Rev. A* **27**, 2110-2113 (1983).

G. F. Albrecht, L. Lund, and D. Smith, "Building a Simple, Reliable, Low-Cost Modelocked System," *Appl. Opt.* **22**, 1276-1280 (1983)

T. Sizer II, J. D. Kafka, I. N. Duling III, C. W. Gabel, and G. A. Mourou, "Synchronous Amplification of Subpicosecond Pulses," *IEEE J. Quantum Electron.* **QE-19**, 506-511 (1983).

Forthcoming Publications

S. Skupsky and K. Lee, "Uniformity of Energy Deposition for Laser-Driven Fusion," accepted for publication by *Journal of Applied Physics*.

B. Yaakobi, H. Kim, J. M. Soures, H. W. Deckman, and J. Dunsmuir, "Sub-Micron X-Ray Lithography Using UV-Laser-Produced Plasma as a Source," accepted for publication by *Journal of Applied Physics*.

R. W. Short and E. A. Williams, "Brillouin Scattering of Multi-Line Laser Light in a Flowing Plasma Corona," accepted for publication by *Physics of Fluids*.

A. Simon, R. W. Short, E. A. Williams, and T. Dewandre, "On the Inhomogeneous Two-Plasmon Instability," accepted for publication by *Physics of Fluids*.

W. Knox, "Interactive Programming Applied to a Jitter-Free Signal-Averaging Streak Camera," accepted for publication in the *Proceedings of the Annual Meeting of the American Chemical Society Symposium on Image Devices in Spectroscopy*.

C. Hanzlik, W. Knox, T. Nordlund, R. Hilf, and S. Gibson, "Picosecond Fluorescence of Hematoporphyrin Derivative, Its Components and Prophyryns," accepted for publication in the *Proceedings of the Clayton Symposium on Prophyrin Localization and Treatment of Tumors*.

J. A. Abate and R. Roides, "Spatially Resolved Absorption and Detection of Microscopic Impurities in Optical Thin Films by Photothermal Detection," accepted for publication in *Journal De Physique Colloques (Photoacoustique)*.

Conference Presentations

M. C. Richardson, S. Skupsky, J. Kelly, L. Iwan, R. Hutchison, R. Peck, R. McCrory, and J. Soures, "Laser Fusion Target Irradiation Uniformity with the 24-Beam OMEGA Facility," presented at the Los Alamos Conference on Optics, Los Alamos, New Mexico, April 1983.

S. L. Gibson, R. Hilf, C. A. Hanzlik, and W. Knox, "Picosecond Fluorescence of Hematoporphyrin Derivative as Separate Components in Aqueous Solution," presented at the Symposium on Prophyrin Localization and Treatment of Tumors, Santa Barbara, California, April 1983.

J. Abate and R. Roides, "Spatially Resolved Absorption and Detection of Microscopic Impurities in Optical Thin Films by Photothermal Deflection," presented at the Third International Topical Meeting on Photoacoustical and Photothermal Spectroscopy, Paris, France, April 1983.

The following presentations were made at the Annual Meeting of the Conference on Lasers and Electro-Optics, Baltimore, Maryland, May 1983:

R. L. McCrory, "Essential Physics and Technology Issues for Direct-Drive Laser Fusion" (invited talk).

G. Albrecht, M. Gruneisen, and D. Smith, "Development and Characterization of a Nd: Phosphate Glass Active Modelocked Q-Switched (AMQ) Oscillator."

W. Seka, L. M. Goldman, R. L. Keck, S. Letzring, M. C. Richardson, J. M. Soures, K. Tanaka, R. S. Craxton, J. Delettrez, E. A. Williams, R. Boni, and D. Quick, "Comparison of Coronal Plasma Parameters in IR-and UV-Laser Plasmas."

M. C. Richardson, J. M. Soures, S. Skupsky, J. Kelly, L. Iwan, and B. Flaherty, "Irradiation Uniformity of Spherical Targets with Multibeam Irradiation."

T. Boehly, L. M. Goldman, W. Seka, and R. S. Craxton, "Hydrodynamic Efficiency of Flat Targets Irradiated with 0.35- μm Laser Light."

G. Mourou, J. Valdmantis, and S. Williamson, "New Approaches to Electrical Transient Sampling Systems with Picosecond Resolution."

T. M. Nordlund, W. Knox, R. Knox, N. E. Geacinton, and J. Breton, "Intensity Dependence of Time-Resolved Chloroplast Fluorescence," presented at the Eleventh Annual Meeting of the American Society for Photobiology, Madison, Wisconsin, June 1983.

C. A. Hanzlik, T. M. Nordlund, W. Knox, S. L. Gibson, and R. Hilf, "Picosecond Fluorescence of Hematoporphyrin Derivative and Its Components in Aqueous Solution," presented at the Eleventh Annual Meeting of the American Society for Photobiology, Madison, Wisconsin, June 1983.

T. G. Dzuira and D. G. Hall, "Bistable Operation of Two Semiconductor Lasers in an External Cavity: Rate Equation Analysis," presented at the Topical Meeting on Optical Bistability, Optical Society of America, University of Rochester, Rochester, New York, June 1983:

The following presentations were made at the Thirteenth Annual Conference on Anomalous Absorption of Electromagnetic Waves, Banff, Alberta, Canada, June 1983.

R. S. Craxton and R. L. McCrory, "Hydrodynamic Calculations of Thermal Self-Focusing in Laser Plasmas."

J. Delettrez, S. Skupsky, D. Shvarts, and R. L. McCrory, "Simulation of Transport Experiments at LLE Using Non-Local Electron Transport Models."

R. Epstein, S. Skupsky, and B. Yaakobi, "Spectral Signatures of Non-Maxwellian and Non-LTE Effects in Thermal Transport Experiments."

S. Skupsky and J. Delettrez, "The Effect of Thermal Flux Saturation on Lateral Heat Transport-A Multi-Group Analysis."

A. Simon, R. W. Short, E. A. Williams, and T. Dewandre, "On the Inhomogeneous Two-Plasmon Instability."

R. W. Short and E. A. Williams, "The Two-Plasmon Instability in a Filament."

E. A. Williams and R. Short, "The Convective Raman Instability."

M. Strauss, G. Hazak, D. Shvarts, and R. S. Craxton, "Magnetic Field Effects on Electron Heat Transport in Laser-Produced Plasmas," presented at CECAM Workshop Proceedings, Orsay, France, October 1982.

B. P. Wittmershaus, T. M. Nordlund, W. H. Knox, R. S. Knox, N. E. Geacintov, and J. Breton, "Intensity Dependence of Time-Resolved Chloroplast Fluorescence," presented at the Eleventh Annual Meeting of the American Society for Photobiology, Madison, Wisconsin, June 1983.

The work described in this volume includes current research at the Laboratory for Laser Energetics which is supported in part by the Empire State Electric Energy Research Company (ESEERCO), the General Electric Company, the New York State Energy Research and Development Authority (NYSERDA), Northeast Utilities, the Standard Oil Company (Ohio), the University of Rochester, and various governmental agencies, including the Department of Energy, the Air Force Office of Scientific Research, the National Institutes of Health, and the National Science Foundation.